Efficient Open Set Single Image Test Time Adaptation of Vision Language Models

Anonymous authors
Paper under double-blind review

Abstract

Adapting models to dynamic, real-world environments characterized by shifting data distributions and unseen test scenarios is a critical challenge in deep learning. In this paper, we consider a realistic and challenging Test Time Adaptation setting, where a model must continuously adapt to test samples that arrive sequentially, one at a time, while distinguishing between known and unknown classes. Existing Test Time Adaptation methods fail to handle this setting due to their reliance on closed-set assumptions or batch processing, making them unsuitable for real-world open-set scenarios. We address this limitation by establishing a comprehensive benchmark for *Open-set Single image Test Time Adaptation using Vision-Language Models*. Furthermore, we propose ROSITA, a novel framework that leverages dynamically updated feature banks to identify reliable test samples and employs a contrastive learning objective to improve the separation between known and unknown classes. Our approach effectively adapts models to domain shifts for known classes while rejecting unfamiliar samples. Extensive experiments across diverse real-world benchmarks demonstrate that ROSITA sets a new state-of-the-art in open-set TTA, achieving both strong performance and computational efficiency for real-time deployment. The code is available anonymously at https://github.com/ostta/ROSITA.git.

1 Introduction

Over the past decade, deep learning has revolutionized computer vision tasks such as image classification, object detection, and segmentation Deng et al. (2009); Ren et al. (2015); He et al. (2017); Everingham et al. (2010). However, these advancements are predominantly realized on the assumption that the training and test data follow the same distribution. In contrast, the real world is dynamic and ever-changing, making such assumptions often untenable. Distribution gaps between training and test data manifest in diverse forms Hendrycks & Dietterich (2019); Peng et al. (2019b), including domain shifts and semantic shifts. Domain shifts could emerge from variations in lighting, weather, camera specifications, or geographical locations between the train and test datasets. Semantic shifts occur when a model, initially trained on a specific set of classes, encounters previously unseen classes during testing. Hence, navigating deep learning models through these dynamic test environments is imperative.

Test Time Adaptation (TTA) addresses this challenge by enabling models to adapt during inference without access to the training data Wang et al. (2021); Schneider et al. (2020); Niu et al. (2022). TTA is characterized by three defining features: (1) no access to source data during adaptation, (2) the absence of ground truth labels for test data, and (3) an online adaptation scenario where test samples are encountered sequentially and accessible only once. These constraints reflect the dynamic and streaming nature of real-world applications. Existing TTA methods have predominantly focused on closed-set scenarios, assuming all test data belongs to known classes. However, these approaches fall short in real-world settings, where models are exposed to unseen categories beyond their training distribution. For example, an autonomous driving system trained to recognize urban vehicles like *car, truck, motorcycle* may incorrectly classify a *bicycle* as a *motorcycle* when deployed in a rural setting. In such scenarios, the model must not only adapt to domain shifts within known categories but also identify unfamiliar elements as *unknown* rather than incorrectly classifying them as part of the known set. This highlights the critical need for **Open-set adaptation** in TTA. In addition, most TTA

methods assume access to batches of test samples Wang et al. (2021); Döbler et al. (2023); Li et al. (2023), which are processed collectively for adaptation. However, this assumption is often impractical in real-time scenarios, where test samples arrive sequentially, one at a time, necessitating efficient **Single image Test Time Adaptation** methods.

Large-scale Vision-Language Models (VLMs), such as CLIP Radford et al. (2021), have demonstrated exceptional generalization capabilities across diverse domains, making them promising candidates for TTA. Recent works like TPTShu et al. (2022) and PromptAlign Samadh et al. (2023) have explored prompt-tuning based adaptation of VLMs at the level of individual test samples, achieving improved zero-shot performance. TDA Karmanov et al. (2024) employs a Training-free Dynamic Adapter to adapt VLMs during test time. However, these methods are restricted to closed-set scenarios and do not address the challenges of more realistic open-set scenarios. Conversely, open-set TTA methods Li et al. (2023); Lee et al. (2023) focus on adapting vision-only backbones (CNNs) trained on specific domains but require batch-wise processing of test samples, making them unsuitable for scenarios where test samples arrive one at a time. The combined challenges of open-set recognition and single-image adaptation remain largely unexplored.

To bridge these gaps, we establish a benchmark for **Open-set Single image Test Time Adaptation (OSTTA)** using VLMs, addressing both open-set recognition and single-image adaptation. We refer to the classes of interest with respect to a particular downstream classification task (say CIFAR-10) as *desired* classes and the rest as *undesired* classes (say CIFAR-100). To identify whether a test sample belongs to a desired or undesired class, we employ a Linear Discriminant Analysis (LDA) Fisher (1936); Li et al. (2023) based class identifier. Samples identified as belonging to the desired classes are then classified accordingly into one of the desired classes. We equip closed-set single image TTA methods with this class identifier to handle open-set scenarios, enabling them to adapt to domain shifts within desired classes while effectively rejecting unfamiliar samples as unknown.

We propose a novel framework termed **ROSITA** designed for OSTTA using VLMs. At the core of this framework is the **ReDUCe** loss, which effectively leverages **Re**liable samples to enhance the separability between **D**esired and **U**ndesired classes through a **C**ontrastiv**e** loss. Additionally, moving beyond existing prompt-tuning approaches, we analyze the optimal set of parameters for adapting VLMs during test-time and identify that adapting LayerNorm parameters offers a lightweight yet effective solution for continuous adaptation. ROSITA dynamically updates these LayerNorm parameters using the ReDUCe loss, enabling it to adapt in open-set environments by accurately identifying unseen classes as "unknown" while maintaining the performance of VLMs on known categories. Our contributions are summarized as follows:

- To the best of our knowledge, we are the first to explore the capability of VLMs in addressing the challenging and realistic problem of *Open-set Single image Test Time Adaptation* (OSTTA), establishing a comprehensive benchmark for this setting.
- Our framework, ROSITA, introduces the ReDUCe loss to enhance separability between desired and undesired class samples, enabling reliable recognition of desired samples under domain shifts while effectively rejecting unfamiliar ones saying *"I don't know"*.
- We conduct a systematic analysis of parameter selection for VLM adaptation during test-time and identify LayerNorm parameters as the optimal choice for lightweight, *continuous adaptation of VLMs*.
- We demonstrate the effectiveness of ROSITA through extensive experiments across diverse domain adaptation benchmarks, simulating real-world test environments with single-domain shifts, continuous and frequent domain shifts, and varying proportions of desired and undesired class samples.

2 Open-set Single image Test Time Adaptation

2.1 Problem Setup

Test stream. The model encounters a single test sample x_t at time t, sampled from $\mathcal{D}_t = \mathcal{D}_d \cup \mathcal{D}_u$ comprising of: (i) Desired class samples: $\mathcal{D}_d = \{x_t; y_t \in C_d\}$, with domain shift and belonging to one of the $\mathcal{C}_d$ desired classes, for example, $C_d = \{car, bus, ..., motorcycle\}$; (ii) Undesired class samples: $\mathcal{D}_u = \{x_t; y_t \in C_u\}$, which have semantic shift (irrelevant classes) such that $C_d \cap C_u = \phi$.

Goal. Given a test sample x_t arriving at time t, the goal is to first recognize if it belongs to a desired class or not, constituting a binary classification task. If x_t is identified as a desired class sample, a subsequent $|C_d|$-way classification is performed. Else, the prediction is "*I don't know*". In essence, the overall process can be viewed as a $|C_d| + 1$ way classification problem.

OSTTA scenarios. We simulate several test scenarios inspired by the real world to evaluate the effectiveness of our method. (1) *Single domain*: We extend the standard TTA scenario where the test samples come from an unseen domain D_d (say *snow* corruption of CIFAR-10C) by incorporating undesired samples D_u (say CIFAR-100C). (2) *Continuously changing domains*: Here, D_t changes with time as $(D_d^1 \cup D_u) \rightarrow (D_d^2 \cup D_u) \ldots \rightarrow (D_d^n \cup D_u)$, where D_d^i is the i^{th} domain encountered. (3) *Frequently changing domains*: Here, we significantly reduce the number of samples per domain in continuous open set TTA. The fewer the samples per domain, the more frequently the test domain changes, simulating very dynamic open-set test scenarios. (4) *Varying sample ratio:* The proportion of samples from C_d and C_u in the test stream is varied.

2.2 Benchmark for OSTTA using VLMs

Here, we describe our motivation for using VLMs for the OSTTA problem and further describe how we establish a benchmark for the same.

CNNs vs VLMs for OSTTA. Test Time Adaptation (TTA) traditionally focuses on CNNs, which are vision-only backbones trained on specific datasets. The goal is to adapt these CNNs to mitigate performance degradation when encountering unseen environments such as noisy or weather-affected conditions. These models usually require specific retraining for each dataset or desired classes. On the other hand, Vision-Language Models (VLMs) like CLIP Radford et al. (2021) are pretrained on diverse image-text pairs from the web. These models demonstrate strong zero-shot generalization capabilities across diverse domains without any specific retraining. This makes VLMs a promising candidate for TTA scenarios. However, defining unseen classes or domains in the context of VLMs is non-trivial due to their exposure to diverse visual data. Although CLIP performs well in zero-shot classification for clean datasets, its performance on corrupted or style-shifted datasets like ImageNet-C/R remains suboptimal Shu et al. (2022), making TTA still relevant. Moreover, CLIP can only classify an image by making a choice from the given set of desired classes. It lacks the ability to explicitly say "*I don't know*" when presented with a sample that does not belong to the set of desired classes, highlighting the need for open-set recognition. Noting these differences and advantages of VLMs over CNNs, we ask these questions: *1) How well can VLMs perform in open-set scenarios? 2) Can they be effectively adapted in a continuous manner? 3) How do we equip VLMs to handle domain shifts within desired classes while accurately rejecting unfamiliar samples?* To address these research questions, we establish a new benchmark and propose a framework termed ROSITA using VLMs.

Classification using VLMs. We evaluate our approach using Vision-Language Models (VLMs) such as CLIP Radford et al. (2021) and MaPLe Khattak et al. (2023) as backbones. CLIP consists of a Vision ($\mathcal{F}_V$) and Text ($\mathcal{F}_T$) encoder trained via contrastive learning on image-text pairs. The MaPLe backbone extends CLIP by incorporating multimodal prompts, enhancing its adaptability for downstream tasks. Given a test image x_t and a set of desired classes $C_d = \{c_1, c_2, \ldots c_N\}$, we construct text-based classifiers using predefined text prompts. Each class name is prepended with the prompt "A photo of a", creating class-specific text inputs $\{\boldsymbol{p}_T, c_i\}$. These inputs are passed through the text encoder to generate text embeddings $\boldsymbol{t}_i = \mathcal{F}_T(\{\boldsymbol{p}_T; c_i\})$ for each $c_i \in C_d$. The resulting classifier consists of text embeddings $\{\boldsymbol{t}_1, \boldsymbol{t}_2, \ldots \boldsymbol{t}_N\}$. Class prediction for a sample x_t is made by identifying the text embedding t_i with the highest similarity to the image feature f_t extracted from the vision encoder.

Baseline Methods. To establish a strong benchmark, we adapt several existing TTA methods designed for closed-set settings to the open-set Single Image TTA scenario. These include ZSEval Radford et al. (2021), TPT Shu et al. (2022), PAlign Samadh et al. (2023), TDA Karmanov et al. (2024) and DPE Zhang et al. (2024). Furthermore, we extend TPT and PAlign to support continuous model updates by adapting prompts, referring to these variants as TPT-C and PAlign-C, respectively. We also adapt open-set TTA approaches originally designed for CNNs, such as (K+1)PC Li et al. (2023) and UniEnt Gao et al. (2024), to work with VLMs. These methods are described in detail in Appendix B. For a fair comparison, all baseline methods are equipped with a simple and efficient class identification mechanism based on the LDA objective Li et al. (2023) to handle the open-set nature of the test stream.

Desired vs Undesired Class Identifier. In an open-set TTA setting, it is crucial for the model to distinguish between samples belonging to desired classes (C_d) and undesired classes (C_u) and appropriately reject samples from C_u. This problem can be viewed as a binary classification problem between desired and undesired samples based on the score s_t. To achieve this, we equip all baseline methods with a parameter-free classifier based on Linear Discriminant Analysis (LDA) Fisher (1936); Li et al. (2023). This classifier uses the similarity score s_t, defined as the maximum cosine similarity between the test sample's image embedding f_t and the text embeddings t_k of the desired classes C_d:

$$s_t = \max_k \text{sim}(f_t, t_k) \tag{1}$$

Rather than relying on a fixed threshold, which can be challenging to define in a streaming TTA scenario, we dynamically determine an optimal threshold using a continuously updated score bank $\mathcal{S}$. This bank stores the most recent $|\mathcal{S}|$ similarity scores, capturing the evolving distribution of the test stream. The optimal threshold τ_t^* is computed using 1D LDA to minimize intra-class variance, as follows:

$$\tau_t^* = \arg\min_\tau \frac{1}{|\mathcal{S}_d|} \sum_{s \in \mathcal{S}_d} (s - \mu_d)^2 + \frac{1}{|\mathcal{S}_u|} \sum_{s \in \mathcal{S}_u} (s - \mu_u)^2 \tag{2}$$

where $\mathcal{S}_d = \{s_i | s_i > \tau, s_i \in S\}$ and $\mathcal{S}_u = \{s_i | s_i < \tau, s_i \in S\}$ represent the scores of samples classified as desired and undesired, respectively, and μ_d and μ_u are their means. Using this threshold, the test sample x_t is classified as:

$$\tilde{y}_t = \begin{cases} \text{desired} & \text{if } s_t \geq \tau_t^* \\ \text{undesired} & \text{if } s_t < \tau_t^* \end{cases} \tag{3}$$

This simple yet effective approach equips the model to handle open-set scenarios by explicitly rejecting undesired samples, thereby ensuring robust performance during adaptation.

We equip all baseline methods (described above) with this LDA objective based desired vs undesired class identifier for a fair comparison in the Open-set Single Image TTA setting. In Appendix C.4, we demonstrate the superior performance of this method compared to naive confidence thresholding. With this comprehensive benchmark established, we now describe our proposed framework, ROSITA, which sets a new standard for Open-set single-image TTA.

3 Proposed ROSITA Framework

Given a single test sample x_t at time t, it is first identified as a desired or undesired class sample as described above. This is important since using undesired class samples can have a negative impact on model adaptation. In this work, we propose a test time objective that can leverage both desired and undesired class samples through feature banks to enhance the discriminability between them.

Reliable samples for TTA. We first identify a test sample x_t as a *reliable desired or undesired class sample* based on its score s_t. As we have access to an approximate distribution of the scores as described in Section 2.2, we leverage the statistics μ_d and μ_u estimated through LDA to identify reliable samples. A test sample x_t is said to be a reliable sample belonging to desired classes C_d if its score $s_t > \mu_d$ and a reliable sample from any of the other classes C_u if its score $s_t < \mu_u$. We leverage **Re**liable samples to differentiate **D**esired vs **U**ndesired class samples through a **C**ontrastiv**e** (**ReDUCe**) Loss for Open-set Single Image Test time Adaptation, as illustrated in Figure 1.

ReDUCe Loss. A contrastive objective typically needs positive and negative features, the goal being to maximize the similarity between a sample and its positives (could be augmentations Chen et al. (2020) or nearest neighbours Dwibedi et al. (2021)), while minimizing its similarity with the negatives. Such objectives (Chen et al., 2020; He et al., 2020; Khosla et al., 2020; Dwibedi et al., 2021) have been extensively used to learn good image representations in a self-supervised way. While self-supervised learning assumes access to abundant data in an offline manner, giving the freedom to carefully choose positives and negatives, this problem is set in an online scenario, where the test samples arrive one at a time and are accessible only at

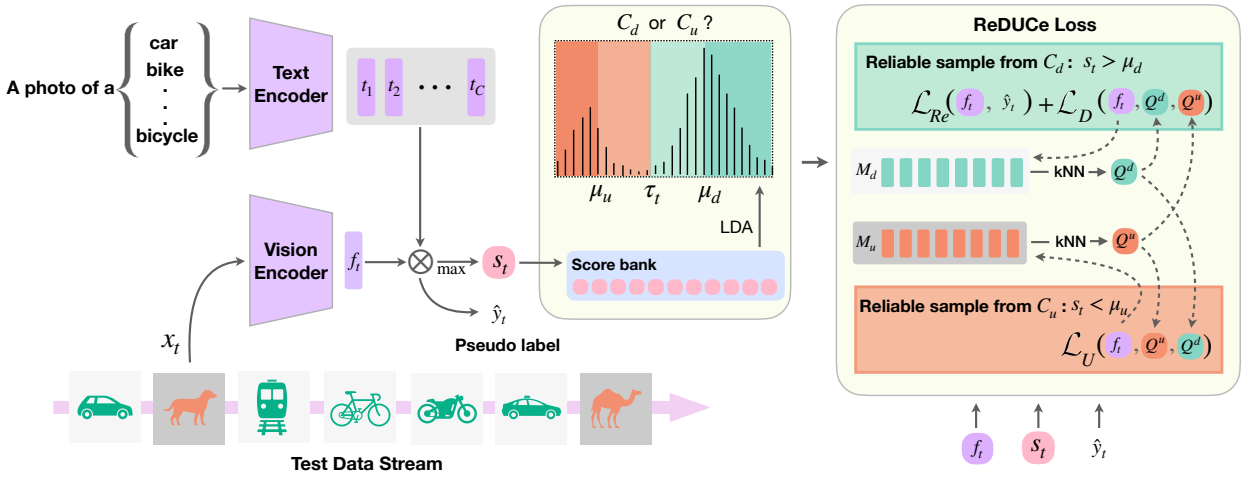

Figure 1: **ROSITA framework:** The test stream with samples from C_d and C_u arrive one at a time. An input image x_t is recognized as a sample from C_d and C_u through an LDA based class identifier. Further, if a test sample is reliable, the respective feature banks are updated and the proposed ReDUCe loss is optimized to update the LayerNorm parameters of the Vision Encoder.

that instant. This challenging setting makes it non-trivial to use objectives like Dwibedi et al. (2021). To circumvent this issue of lack of abundant test data, we propose to store two dynamically updated feature banks $\mathcal{M}_d$ and $\mathcal{M}_u$ of sizes N_d and N_u, to store the features of reliable samples from C_d and C_u respectively. We propose a ReDUCe objective to contrast a reliable sample from C_d by choosing its positives and negatives as the K nearest neighbours from $\mathcal{M}_d$ and $\mathcal{M}_u$ respectively and vice versa for a reliable sample from C_u. The buffer size for $\mathcal{M}_d$ is set as $|C_d| \times K$, where $|C_d|$ is the number of desired classes and K is the number of neighbours retrieved. The feature banks $\mathcal{M}_d$ or $\mathcal{M}_u$ are updated with a feature f_t if it is detected as a reliable sample from C_d or C_u.

We fetch the K nearest neighbours of a reliable test sample x_t from each feature bank as follows.

$$Q_d = \text{kNN}(f_t; \mathcal{M}_d); \quad Q_u = \text{kNN}(f_t; \mathcal{M}_u) \tag{4}$$

Case 1: Reliable sample from C_d. If a test sample is identified as a reliable sample from C_d, we use a reliable pseudo-label loss on the sample x_t and its augmentation $\tilde{x}_t$ as follows:

$$\mathcal{L}_{Re} = \mathcal{L}_{CE}(x_t, \hat{y}_t) + \mathcal{L}_{CE}(\tilde{x}_t, \hat{y}_t); \quad \hat{y}_t = \text{argmax}_i \, \text{sim}(f_t, t_i) \tag{5}$$

where sim represents cosine similarity. Further, we also propose to use a contrastive objective to enhance the clustering of desired class samples while pushing them apart from the undesired class samples.

As we aim to correctly classify the desired class samples, we select positives z^+ from Q_d if its prediction y^+ matches with $\hat{y}_t$. The features Q_u consisting of its kNN from M_u act as its negatives. The following is the ReDUCe loss for a reliable sample from C_d:

$$\mathcal{L}_D = -\frac{1}{K^+} \sum_{z^+ \in Q^d} \mathbf{1}(y^+ = \hat{y}_t) \log \frac{\exp\left(\text{sim}\left(f_t, z^+\right)/\tau\right)}{\sum\limits_{z^- \in Q^u} \exp(\text{sim}(f_t, z^-)/\tau)} \tag{6}$$

where $K^+ = \sum_{z^+ \in Q^d} \mathbf{1}(y^+ = \hat{y}_t)$, is the number of neighbours positively matched with $\hat{y}_t$.

Case 2: Reliable sample from C_u. If a test sample is identified as a reliable sample from C_u, we use the following contrastive objective by selecting positives z^+ from Q_u and negatives z^- from Q_d:

$$\mathcal{L}_U = -\frac{1}{K} \sum_{z^+ \in Q_u} \log \frac{\exp\left(\text{sim}\left(f_t, z^+\right)/\tau\right)}{\sum\limits_{z^- \in Q_d} \exp(\text{sim}(f_t, z^-)/\tau)} \tag{7}$$

Table 1: Results with ImageNet-C/R as desired class data D_d, MNIST and SVHN for D_u.

	Method	IN-C/MNIST			IN-C/SVHN			IN-R/MNIST			IN-R/SVHN		
		AUC ↑	FPR ↓	HM ↑	AUC ↑	FPR ↓	HM ↑	AUC ↑	FPR ↓	HM ↑	AUC ↑	FPR ↓	HM ↑
CLIP	ZS-Eval	93.39	55.52	41.43	85.89	72.91	40.83	91.27	91.09	71.50	90.43	75.04	71.66
	TPT	93.12	58.01	42.21	85.43	74.47	40.95	91.25	91.23	71.98	90.43	74.98	72.36
	TPT-C	56.57	99.12	6.19	11.38	100.00	7.24	82.81	85.79	68.25	80.94	80.03	69.18
	(K+1) PC	95.76	10.43	42.95	87.75	26.23	38.50	97.46	11.78	81.51	97.55	11.17	80.39
	UniEnt	94.19	46.98	41.53	87.56	67.03	41.10	91.64	88.67	71.73	90.86	71.53	71.96
	TDA	90.54	76.23	43.66	86.76	75.45	43.07	91.79	87.83	71.56	90.67	75.41	71.48
	DPE	87.92	91.94	42.87	82.96	77.90	41.93	92.13	81.09	71.39	90.86	73.30	70.64
	ROSITA	**99.52** +6.13	**4.06** +51.46	**48.53** +7.10	**98.34** +12.45	**10.21** +62.70	**46.32** +5.49	**99.44** +8.17	**4.29** +86.80	**83.53** +12.03	**98.62** +8.19	**9.08** +65.96	**80.75** +9.09
MAPLE	ZS-Eval	81.49	92.95	41.70	83.26	71.15	42.77	90.15	83.54	74.42	92.74	65.70	75.71
	TPT	81.38	93.17	39.92	83.18	71.52	40.93	90.14	83.58	74.00	92.74	65.68	75.23
	TPT-C	83.25	87.60	42.81	83.18	70.60	42.86	90.35	81.49	74.73	92.79	65.20	75.59
	PAlign	81.38	93.17	41.32	83.18	71.52	42.30	90.14	83.58	74.66	92.74	65.68	75.93
	PAlign-C	71.22	86.32	27.14	32.17	94.32	15.44	92.20	59.70	75.23	93.54	54.59	75.67
	(K+1)PC	98.58	3.35	48.69	77.17	39.74	38.10	99.01	3.16	84.23	95.14	13.77	80.16
	UniEnt	81.53	93.45	41.50	83.41	70.84	42.78	90.14	83.49	74.48	90.14	83.49	74.48
	TDA	76.79	99.02	42.98	82.46	91.75	44.63	90.43	86.56	73.66	92.92	64.63	74.16
	DPE	73.97	99.59	41.39	80.06	87.10	44.05	90.44	78.77	72.67	93.48	55.74	76.74
	ROSITA	**99.56** +18.07	**1.66** +91.29	**51.30** +9.60	**98.68** +15.42	**5.09** +66.06	**50.67** +7.90	**99.39** +9.24	**2.95** +80.59	**84.70** +10.28	**97.85** +5.11	**12.98** +52.72	**83.07** +7.36

The LayerNorm parameters of the Vision Encoder are updated to minimize the following test time objective to adapt the model one sample at a time in an online manner:

$$\mathcal{L}_{ReDUCe} = \begin{cases} \mathcal{L}_{Re} + \mathcal{L}_D & \text{if} \quad s_t > \mu_d \\ \mathcal{L}_U & \text{if} \quad s_t < \mu_u \end{cases} \tag{8}$$

This objective improves the proximity between the test sample and its positives, suitably chosen based on its score s_t, while also pushing apart the test sample and its negatives. This collectively encourages the model to adapt such that each of the desired classes and undesired classes are clustered and farther apart from each other, improving the overall classification performance of C_d and C_u. We now perform Gradient Analysis on the loss function and theoretically justify how the proposed ReDUCe loss helps in enhancing the discriminability between desired and undesired class samples.

3.1 Gradient Analysis of the proposed REDUCE Loss

The key to understanding the behavior of the contrastive loss is to analyze its gradient. The softmax term in the denominator encourages f_t to have lower similarity with negative samples, and the numerator encourages f_t to have higher similarity with positive samples. We compute the gradient of the loss components L_D and L_U of the ReDUCe loss with respect to f_t (Appendix A).

$$\begin{aligned} \frac{\partial \mathcal{L}_D}{\partial f_t} &= -\frac{1}{K^+} \sum_{z^+ \in Q^d} \mathbf{1}\left(y^+ = \hat{y}_t\right) \cdot \frac{1}{\tau} \left(z^+ - \sum_{z^- \in Q^u} p\left(z^-\right) z^- \right) \\ \frac{\partial \mathcal{L}_U}{\partial f_t} &= -\frac{1}{K} \sum_{z^+ \in Q^u} \frac{1}{\tau} \left(z^+ - \sum_{z^- \in Q^d} p\left(z^-\right) z^- \right) \end{aligned} \tag{9}$$

where $p\left(z^-\right)$is the softmax probability of the negative samples defined as

$$p\left(z^-\right) = \frac{\exp\left(\text{sim}\left(f_t, z^-\right)/\tau\right)}{\sum_{z' \in Q^-} \exp\left(\text{sim}\left(f_t, z'\right)/\tau\right)} \tag{10}$$

where Q^- is Q^u for $\mathcal{L}_D$ and Q^d for $\mathcal{L}_U$. The gradient of these contrastive loss formulations drives the following behavior in this context:

1. **Attraction to positive neighbors.** In the gradient of $\mathcal{L}_D$, the first term pulls the test feature f_t towards its positives $z^+ \in Q^d$, representing the attraction force that encourages samples from desired classes to form $|C_d|$ tight clusters as the positives are chosen such that $\hat{y}_t = y^+$. Similarly, in the gradient of $\mathcal{L}_U$, the first term pulls f_t towards its positives $z^+ \in Q^u$, encouraging all samples from C_u to cluster together.

2. **Repulsion from negative neighbors.** The second term $p\left(z^-\right) z^-$ in the gradient pushes the test feature f_t away from its negatives $z^- \in Q^-$ (Q^- is Q^u for $\mathcal{L}_D$ and Q^d for $\mathcal{L}_U$). The strength of the repulsion is controlled by the softmax probability $p(z^-)$, where more similar negatives exert a stronger repulsive force on f_t, increasing the separation between samples from C_d and C_u. As the negatives selected are its K nearest neighbours of the opposite type, they are, in fact, hard negatives. Further, the contrastive objective inherently models the degree of hardness through the means of this probability $p(z^-)$. The closer the hard negative, the stronger the repulsion force.

We now present our analysis on the parameter choices for continuous adaptation of VLMs.

4 Analysis on parameters for Continuous Adaptation of VLMs

Test time adaptation methods using CNNs Wang et al. (2021); Schneider et al. (2020); Liang et al. (2020); Chen et al. (2022) successfully leverage test domain data arriving in an online manner (in batches) to continuously update the model. In this work, we study TTA of VLMs like CLIP, which has only been explored very recently Shu et al. (2022); Karmanov et al. (2024); Zhang et al. (2024) by adapting prompts independently for each image. While these methods show promise for on-the-fly adaptation in a zero-shot framework, it is not clear whether they can leverage the online data stream to continuously update the model parameters. Based on the evidence in prior TTA works (Wang et al., 2021; Chen et al., 2022), we analyze two aspects of VLMs for the TTA task: (1) Here, we question if VLMs can be continuously adapted in a similar manner, but using only a single test image at a time; (ii) If so, are prompts (Shu et al., 2022) the best parameters to continuously update?

Experiment. We choose six different parameter groups: (1) Prompts, (2) LayerNorm parameters (Zhao et al., 2023), (3) Full network (4) First Attention Block of ViT (5) Last Attention Block of ViT (6) Prompts+LayerNorm(LN). We perform *single image TTA in a closed set scenario* on CIFAR-10C, by continuously adapting each of these parameter groups of CLIP, using reliable entropy loss, $L_{TTA} = \mathbf{1}(s_t > \tau)\mathcal{L}_{ent}(x_t)$, which is commonly used in several TTA methods (Wang et al., 2021; Niu et al., 2022) and VLM based prompt tuning methods like TPT, PAlign. Here, x_t and s_t refer to the test sample and its confidence, respectively. τ is the confidence threshold used to select reliable samples Niu et al. (2022) for the model update, which we set to 0.7 in this analysis.

Observations. We find that continuous model adaptation can indeed improve VLMs performance based on our empirical analysis (Figure 2). (1) Using a high learning rate of 10^{-2} for any parameter group results in a severe drop in accuracy compared to the zero-shot performance of CLIP in this extreme setting of continuous single image model update. (2) The other extreme of low learning rate of 10^{-6} performs at par with ZSEval for all parameter groups, suggesting the model has not sufficiently changed. (3) Updating the Full Network results in an accuracy of about 10% across all learning rates, suggesting that giving the highest flexibility can cause the model to lose the inherent generalization ability of the VLM. (4) Early attention layers can potentially be updated. However, they are more sensitive to learning rate and optimizer choice (Appendix C.5). Also, prompt updates are more expensive as the compute scales with the number of classes, making them less suitable for continuous adaptation (Table 4). (5) We find that tuning the LayerNorm parameters of the Vision encoder (which account for just 0.032% of the total parameters) offers the best balance between performance and complexity.

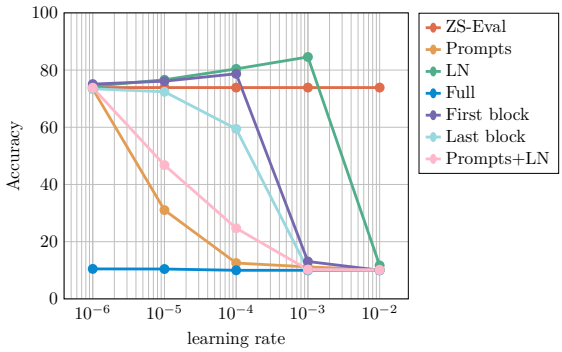

Figure 2: Accuracy on fine-tuning different parameter groups for single image TTA.

Adapting Image encoder vs Text classifiers: Most existing TTA approaches Schneider et al. (2020); Wang et al. (2021); Chen et al. (2022) focus on adjusting image representations for domain shifts during test time while keeping the classifiers fixed. This strategy helps retain class discriminative information. In contrast, in TPT and PAlign, the text-based classifiers that depend on learnable prompts are updated based on single images. While this does not impact zero-shot evaluation (since the model resets after each image), it can be detrimental during continuous updates.

Based on this analysis, we freeze the text-based classifiers and modify only the image representations using LayerNorm affine parameters. The rationale behind this approach is that text representations can be inherently more robust across domains. Text embeddings, often derived from a wide range of linguistic contexts, capture semantic meanings that are less susceptible to variations in visual data. Therefore, adapting the image encoder allows for more effective handling of domain shifts while retaining the class-level discriminative information from the text modality. This ensures that the model can be updated continuously without the need for resets, ultimately enhancing its performance in dynamic, real open-set environments.

5 Experiments

Datasets. We experiment with a diverse set of datasets to choose desired class data D_d and undesired class data D_u. For D_d, we use CIFAR-10C Hendrycks & Dietterich (2019), CIFAR-100C Hendrycks & Dietterich (2019), ImageNet-C Hendrycks & Dietterich (2019) from the corruption category and ImageNet-R Hendrycks et al. (2021), VisDA Peng et al. (2017) and the Clipart, Painting, Sketch domains from DomainNet Peng et al. (2019a) as style transfer datasets. We introduce samples from MNIST LeCun et al. (1998), SVHN Netzer et al. (2011), CIFAR-10/100C Hendrycks & Dietterich (2019) and TinyImageNet Le & Yang (2015) datasets as D_u in the test stream. We describe the datasets in detail in the Appendix B.3.

Table 2: Acc_{HM} on VisDA dataset and Clipart, Painting, Sketch domains from DomainNet as D_d and MNIST as D_u.

Method	VisDA	Clipart	Painting	Sketch
ZSEval	78.28	50.22	47.81	48.59
TPT	78.42	57.71	49.73	54.67
TPT-C	75.35	57.57	49.31	54.41
(K+1)PC	90.35	71.21	70.61	67.21
UniEnt	78.09	57.88	49.75	54.76
TDA	76.85	61.04	51.20	55.26
DPE	53.67	54.52	47.91	32.18
ROSITA	90.64 **+12.36**	71.40 **+21.18**	70.89 **+23.08**	67.35 **+18.76**

Implementation Details. We use CLIP and MaPLe backbones with ViT-B16 architecture. For ROSITA, we use SGD optimizer with a learning rate of 0.001 to update the LayerNorm parameters of the Vision encoder. We set size of the score bank $\mathcal{S}$ to 512, number of neighbours K to 5. The size of feature bank M_d is set as $K \times C_d$ and that of M_u to 64. Implementation details for all the baseline methods are presented in Appendix B.4 *We equip all methods with the same C_d vs C_u class identifier described in Section 2.2.* All experiments are done on a single NVIDIA A6000 GPU.

Evaluation Metrics. We employ standard metrics, namely Area Under the Receiver Operating Characteristic Curve (AUROC) and False Positive Rate at a True Positive Rate of 95% (FPR95), from the OOD detection literature Lee et al. (2023); Li et al. (2023); Wang et al. (2023). Additionally, we compute the classification accuracy for desired class samples (Acc_D) and the binary classification accuracy for correctly recognizing samples from C_u (Acc_U) as defined below. To gauge the overall performance, we compute Acc_{HM} (HM), representing the harmonic mean of Acc_D and Acc_U, which serves as a comprehensive metric capturing the trade-off between Acc_D and Acc_U. Here, we summarily report AUROC (AUC), FPR95 (FPR) and Acc_{HM} (HM) for all the datasets.

$$Acc_D = \frac{\sum_{(x_i,y_i)\in\mathcal{D}_d} \mathbf{1}\left(y_i = \hat{y}_i\right) \cdot \mathbf{1}\left(y_i \in C_d\right)}{\sum_{(x_i,y_i)\in\mathcal{D}_d} \mathbf{1}\left(y_i \in C_d\right)}; \quad Acc_U = \frac{\sum_{(x_i,y_i)\in\mathcal{D}_u} \mathbf{1}\left(\hat{y}_i \in C_u\right) \cdot \mathbf{1}\left(y_i \in C_u\right)}{\sum_{(x_i,y_i)\in\mathcal{D}_u} \mathbf{1}\left(y_i \in C_u\right)}$$

Table 3: Results with CIFAR-10C/100C as desired class data D_d and four other datasets as D_u.

		Method	MNIST			SVHN			Tiny-ImageNet			CIFAR-100C/10-C		
			AUC ↑	FPR ↓	HM ↑	AUC ↑	FPR ↓	HM ↑	AUC ↑	FPR ↓	HM ↑	AUC ↑	FPR ↓	HM ↑
CIFAR-10C	CLIP	ZS-Eval	91.91	85.04	75.57	89.93	64.20	74.08	91.33	27.07	74.63	82.57	67.92	68.89
		TPT	91.89	85.55	75.81	89.93	64.41	74.36	91.31	27.23	75.17	82.57	68.06	69.17
		TPT-C	81.64	67.53	74.86	58.48	71.72	48.26	74.08	61.45	49.88	61.45	94.30	46.10
		(K+1)PC	98.05	12.50	83.27	80.74	50.33	70.10	87.09	52.29	73.98	62.55	91.68	56.46
		UniEnt	91.98	85.2	75.62	89.97	64.38	74.18	91.40	26.96	74.73	82.59	68.14	68.98
		TDA	92.94	71.11	77.06	92.02	52.68	76.64	91.68	25.37	75.94	83.54	66.06	70.13
		DPE	46.97	99.10	27.60	84.15	85.24	68.52	89.92	31.30	69.90	79.18	75.06	62.34
		ROSITA	**99.10**	**7.63**	**84.17**	**94.79**	**32.59**	**78.80**	**96.43**	**12.10**	**80.06**	**82.99**	**62.89**	**69.56**
			+7.19	**+77.41**	**+8.60**	**+4.86**	**+31.61**	**+4.72**	**+5.10**	**+14.97**	**+5.43**	**+0.42**	**+5.03**	**+0.6**
	MAPLE	ZS-Eval	98.48	3.77	83.63	98.34	**7.86**	83.57	90.86	27.54	76.04	86.14	52.08	71.76
		TPT	98.15	5.67	81.56	98.34	7.89	82.73	90.86	27.61	75.46	86.15	52.14	70.94
		TPT-C	98.56	**3.74**	83.51	98.32	8.18	83.47	91.18	26.93	76.31	86.50	50.56	71.07
		PAlign	98.15	5.67	82.24	**98.34**	7.90	83.51	90.86	27.60	75.98	86.15	52.18	71.52
		PAlign-C	98.56	3.74	83.49	98.32	8.13	83.46	91.18	26.90	76.30	86.50	50.58	71.04
		(K+1)PC	98.34	9.63	86.52	71.01	78.78	68.70	71.20	85.81	68.29	62.35	88.44	61.89
		UniEnt	98.17	5.49	82.64	98.35	7.85	83.65	90.90	27.41	76.08	86.16	51.91	71.72
		TDA	98.42	4.13	81.97	98.60	6.20	83.95	91.27	27.00	76.84	86.72	51.40	72.61
		DPE	83.82	92.73	55.52	97.42	12.95	79.41	89.10	31.13	74.32	73.57	73.67	53.64
		ROSITA	**99.34**	5.22	**87.63**	97.80	13.15	**84.17**	**91.67**	**25.31**	**77.67**	**86.82**	**50.33**	**73.15**
			+0.86	**-1.45**	**+4.00**	**+0.54**	**-5.29**	**+0.60**	**+0.81**	**+2.23**	**+1.63**	**+0.68**	**+1.75**	**+1.39**
CIFAR-100C	CLIP	ZS-Eval	77.78	99.93	48.39	64.70	98.68	45.85	67.31	73.89	45.80	63.28	93.25	44.04
		TPT	77.76	99.94	48.33	64.71	98.63	45.85	67.28	73.82	45.93	63.26	93.20	44.02
		TPT-C	51.57	100.00	27.04	9.40	99.98	5.74	59.74	79.76	18.41	55.86	**86.35**	13.64
		(K+1)PC	96.89	12.15	59.72	75.24	51.64	43.73	41.84	99.61	31.83	54.02	93.93	32.00
		TDA	80.33	99.57	46.52	71.77	96.11	46.01	70.70	69.63	47.52	66.07	91.90	45.79
		UniEnt	77.94	99.93	48.32	64.78	98.61	45.84	67.40	73.77	45.83	63.28	93.18	44.04
		DPE	67.06	99.88	42.54	43.23	99.79	35.69	61.42	80.62	42.80	60.08	92.80	42.21
		ROSITA	**96.07**	**19.28**	**57.34**	**82.09**	**64.64**	**48.17**	**83.55**	**50.76**	**55.88**	**68.54**	89.71	**47.98**
			+18.29	**+80.65**	**+8.95**	**+17.39**	**+34.04**	**+2.32**	**+16.24**	**+23.13**	**+10.08**	**+5.26**	**-3.54**	**+3.94**
	MAPLE	ZS-Eval	87.43	64.19	54.97	92.98	40.51	56.42	68.80	74.35	48.24	66.93	87.94	46.06
		TPT	87.42	64.09	53.09	92.97	40.44	54.37	68.80	**74.20**	46.97	66.93	87.95	44.38
		TPT-C	87.65	63.08	55.14	93.09	40.30	56.31	68.85	74.71	48.53	66.97	87.94	46.30
		PAlign	87.42	64.11	53.98	92.97	40.48	55.37	68.80	74.23	47.69	66.93	87.93	45.16
		PAlign-C	88.25	57.31	55.69	93.45	39.39	57.39	68.76	78.12	48.15	66.82	87.80	47.01
		(K+1)PC	96.49	9.42	62.97	65.73	78.63	32.60	42.94	99.95	27.52	53.48	94.26	34.70
		TDA	89.82	52.24	55.46	95.04	30.76	59.51	72.05	71.83	49.19	69.12	87.36	49.06
		UniEnt	87.40	64.02	54.86	92.99	40.36	56.42	68.84	74.26	48.41	66.93	87.96	46.09
		DPE	39.05	98.88	33.66	84.29	76.13	52.20	63.74	82.75	45.74	65.61	90.67	46.36
		ROSITA	**97.04**	**11.01**	**62.06**	**96.26**	**20.99**	**59.25**	**70.37**	77.00	**48.68**	**69.57**	**83.61**	**48.80**
			+9.61	**+53.18**	**+7.09**	**+3.28**	**+19.52**	**+2.83**	**+1.57**	**-2.65**	**+0.44**	**+2.64**	**+4.33**	**+2.74**

6 Research Questions

1) How does ROSITA perform in comparison with prior methods in OSTTA setting?

We observe, from Table 1, 2, 3 that TPT and PAlign perform similar to ZSEval in most datasets, as the prompts are reset after every single image update. On continuously updating prompts in TPT-C and PAlign-C, we observe a reduction in HM compared to ZS-Eval. The effect is more severe with CLIP when compared to MaPLe, as only the text prompts are updated keeping the vision encoder fixed (as also observed in Section 4). (K+1)PC and UniEnt, where LayerNorm tuning is done, perform better than prompt tuning methods. However, **ROSITA**, being equipped with a carefully designed objective to better discriminate between samples from C_d and C_u samples (Figure 3), results in overall better metrics in general.

2) How does ROSITA perform in different real-world inspired OSTTA scenarios?

(a) Continuously changing domains: We sequentially present 15 corruptions from CIFAR-10C, which form the domain D_d, alongside samples from four other datasets D_u. **(b) Frequently changing domains:** To further simulate more dynamic test environments, for CIFAR-10C/MNIST, we reduce the number of samples per corruption to 100, 250, 500, and 1000 in the continuously changing domain open-set TTA scenario. Reducing the sample count per corruption causes more frequent domain changes, increasing the challenge for adaptation. **(c) Varying ratio of samples belonging to classes C_d vs C_u:** We simulate real-world scenarios using the CIFAR-10C/MNIST dataset by varying the ratio of samples from the known classes C_d

Table 5: Performance in different Open set TTA scenarios.

Method	(a) Continuously changing domains				(b) Frequently changing domains				(c) Varying ratio of C_d/C_u			
	CIFAR-10C				No. of samples per corruption				Ratio			
	SVHN	MNIST	Tiny	C-100C	100	200	500	1000	0.2	0.4	0.6	0.8
ZSEval	64.33	64.04	66.50	58.49	61.41	61.87	61.42	63.30	75.56	75.59	75.57	75.56
TPT	64.26	64.03	66.50	58.47	61.33	62.32	61.59	63.24	75.67	75.75	75.81	75.83
TPT-C	33.05	46.44	59.38	37.24	60.62	61.30	57.16	34.88	72.70	74.31	74.79	75.16
(K+1)PC	65.13	62.52	66.93	57.46	60.90	60.76	61.40	63.26	62.31	68.85	81.70	82.90
TDA	66.02	66.44	67.64	59.44	60.17	61.43	63.22	64.82	72.45	75.04	77.54	77.91
DPE	23.36	50.12	58.96	35.56	47.48	46.22	39.83	46.52	65.67	66.12	56.38	29.98
ROSITA	**66.86**	**65.26**	**68.89**	**59.16**	**61.64**	**66.82**	**67.97**	**73.24**	**82.96**	**83.97**	**84.51**	**84.37**

versus unknown classes C_u in the test stream by varying this ratio as 0.2, 0.4, 0.6, and 0.8. From results in Table 5, we observe that **ROSITA** demonstrates consistent superiority across all three open-set TTA scenarios, showcasing its capability to adapt effectively to both continuously and frequently changing domains, as well as varying class distributions.

3) What is the importance of each loss component proposed in ROSITA?

We observe that only using $\mathcal{L}_{Re}$ or $\mathcal{L}_D$ improves the metrics for CIFAR-10C dataset. For ImageNet-R (IN-R) as D_d, using $\mathcal{L}_{Re}$ or $\mathcal{L}_D$ is observed to increase FPR and decrease HM. IN-R has 200 classes making it a more challenging and confusing task compared to CIFAR-10C. This decrease in performance for IN-R can be attributed to the misclassification of some samples from C_u as reliable desired class samples, increasing the confusion between C_d and C_u classes. Using $\mathcal{L}_U$ significantly reduces the confusion between samples from C_d and C_u, shown by the significant drop in FPR compared to ZSEval. The contrastive objectives $\mathcal{L}_D$ and $\mathcal{L}_U$ to separate the two types of samples, in conjunction with reliable pseudo label loss $\mathcal{L}_{Re}$ which aids to improve the $|C_d|$-way classification of desired class samples, gives the overall best results.

Table 4: Ablation study on loss components.

$\mathcal{L}_{Re}$	$\mathcal{L}_D$	$\mathcal{L}_U$	CIFAR-10C/MNIST			IN-R/MNIST		
			AUC ↑	FPR ↓	HM ↑	AUC ↑	FPR ↓	HM ↑
✗	✗	✗	91.91	85.04	75.57	91.27	91.09	71.5
✓	✗	✗	95.29	30.82	80.97	81.07	99.02	64.32
✗	✓	✗	95.23	28.91	79.71	87.73	94.67	67.28
✗	✗	✓	98.61	12.73	79.84	99.39	4.81	80.82
✓	✓	✗	96.23	22.73	79.24	76.78	99.22	62.54
✓	✗	✓	98.69	12.06	82.98	99.34	4.67	82.98
✗	✓	✓	**99.27**	**4.15**	80.69	**99.48**	4.40	81.92
✓	✓	✓	99.10	7.63	**84.17**	99.44	**4.29**	**83.53**

4) What is the role of using reliable samples for OSTTA in ROSITA?

To understand the role of selecting reliable samples for TTA, we do a simple experiment where we only use the threshold τ_t to distinguish between C_d and C_u samples. For all the samples with $s_t > \tau_t$ identified to belong to C_d, we perform TTA using $\mathcal{L}_{Re} + \mathcal{L}_D$ (Equation 6). Similarly, we use L_U (Equation 7) for all samples identified to belong to C_u based on the criterion $s_t < \tau_t$. From the results in Table 6, we see that, for CIFAR-10C and VisDA, this case performs slightly better than our case(last row in Table 6) where TTA is performed only on reliable samples. CIFAR-10C and VisDA dataset have 10 and 12 classes of interest respectively. The zero shot performance of these datasets being good, as the class confusion is less, using all samples for TTA can be helpful. On the other hand, the classification in CIFAR-100C, ImageNet-C and ImageNet-R is harder, due the inherent confusion arising due to the large number of classes. Using non reliable test samples, with scores in the range $\mu_u < s_t < \mu_d$ can adversely affect the adaptation process. Hence, using only reliable samples for TTA performs better for these datasets as seen in Table 6). In a real world test time adaptation scenario, where we have no prior information about the difficulty of the classification task, in terms of severity of domain shift and class confusion, it is desirable to only use reliable samples for model updates.

Table 6: Need for Reliable samples.

Thresholds	D_u: MNIST				
$\tau_u/\tau_t/\tau_d$	C-10C	C-100C	IN-C	IN-R	VisDA
$\tau_t/\tau_t/\tau_t$	**84.99**	55.16	44.05	83.28	**91.24**
$\mu_u/\tau_t/\mu_d$	84.17	**57.34**	**48.53**	**83.53**	90.64

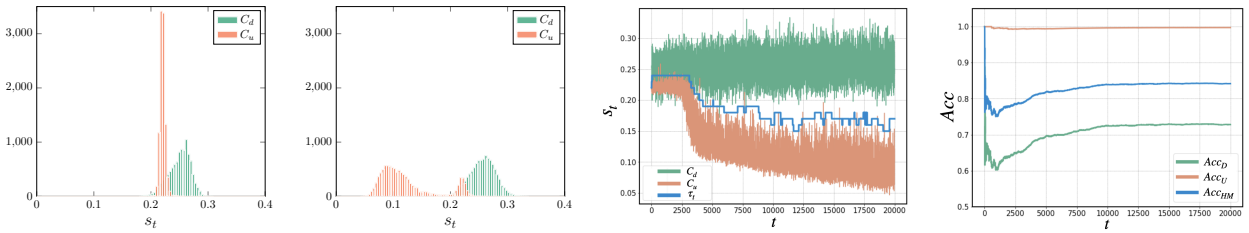

(a) ZSEval (b) ROSITA (c) scores with time (d) Accuracy with time

Figure 3: Histograms of the scores s_t for ZS-Eval (a) and ROSITA (b) on CIFAR-10C/MNIST dataset. (c) Change in scores for C_d and C_u class samples, the best threshold with time t; (d) Accuracy metrics measured for samples seen until time t. Using the LDA-based class identifier with ROSITA, samples from C_d and C_u separate them better, and the accuracy metrics improve with time.

5) How do the scores s_t and the performance of ROSITA vary with time?

We plot the scores s_t of samples from C_d and C_u over time, along with the threshold τ_t, in Figure 3c using ROSITA. Initially, the scores of C_d and C_u overlap significantly ($t < 2500$), leading to unstable performance as shown in Figure 3d. During this phase, the threshold τ_t tends to classify most C_u samples correctly, resulting in high Acc_U but low Acc_D, as many desired class samples are incorrectly rejected. However, as the ReDUCe loss progressively improves class separability, τ_t adapts to the evolving score distribution, enhancing discrimination between C_d and C_u. This refinement stabilizes the model's performance, yielding steady improvements in Acc_D and Acc_{HM} for $t > 2500$. The instability observed for $t < 1500$ is attributed to the initial learning process and the small sample size, as accuracy is measured on the cumulative number of samples seen up to time t, which is exactly t in single image TTA.

6) How does ROSITA fare in terms of memory required?

Prompt tuning methods like TPT, PAlign do not require any memory buffer. TDA requires a memory buffer of size $(|C_d| \times (3+2)) \times F$ to store 3 features per desired class in the positive cache and 2 features per class in the negative cache. DPE requires a memory buffer of size $(|C_d| \times 3) \times F$ to store 3 features per desired class. ROSITA requires a memory buffer of size $(|C_d| \times K + |M_u|) \times F$ for the two feature banks. For a ViT-B16 ($F = 512$) model with ImageNet-C ($|C_d| = 1000$), the required memory buffer size is $5 \times 1000 \times 512 + 64 \times 512$ (10.89MB). *The memory to store these features and computation required to compute feature similarity is as lightweight as performing a forward pass through a simple linear layer, demonstrating the memory and computational efficiency of* **ROSITA** *for real time applications.*

Table 7: Memory overhead in ROSITA.

Dataset	$\lvert C_d \rvert$	No. of features	Memory (in MB)
CIFAR-10C	10	5x10+64	0.758
VisDA	12	5x12+64	0.778
CIFAR-100C	100	5x100+64	1.679
ImageNet-R	200	5x200+64	2.703
ImageNet-C	1000	5x1000+64	10.89

7) How does ROSITA fare in terms of the GPU memory required and inference time?

The GPU memory and time taken (secs/image) for prompt tuning methods TPT scales with the number of classes, as more memory is required to store the intermediate activations and gradients to backward pass through the text encoder. On the other hand, ROSITA requires two forward passes and one backward pass through the vision encoder for reliable test samples. Figure 4 compares the GPU memory and time complexity of ZS-Eval, TPT, and ROSITA representative of training-free methods (ZS-Eval, TDA), prompt-tuning (TPT/-C, PAlign/-C), and LayerNorm-tuning((K+1)PC, UniEnt, ROSITA) based methods in Figure 4. For e.g., for ImageNet-C dataset with 1000 classes, ZSEval, TPT and ROSITA

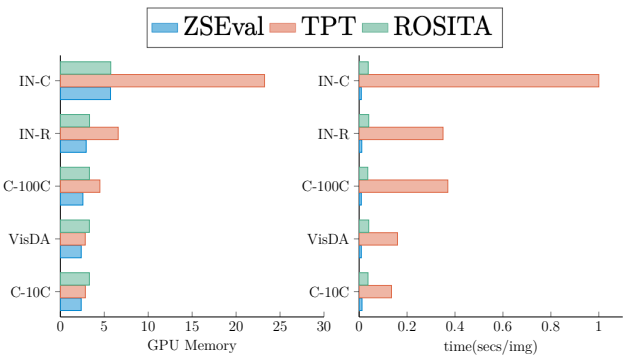

Figure 4: Complexity Analysis of different methods.

require 5.71 GB, 23.24 GB and 5.73 GB GPU memory to perform a single image based model update. Thus, **ROSITA** achieves computational efficiency comparable to training-free methods while being far more efficient than prompt-tuning approaches. Despite its minimal computational overhead, ROSITA offers substantial performance gains, providing a balanced trade-off between efficiency and effectiveness for OSTTA scenarios.

8) What are the key factors distinguishing ROSITA from prior works?

1. *Enhanced Use of LDA Statistics to identify Reliable samples*: Apart from the threshold τ_t, ROSITA leverages the score statistics μ_d and μ_u provided by the LDA class identifier, combined with the novel ReDUCe loss function, to adapt the model. This synergy enhances the discriminability between desired (C_d) and undesired (C_u) class samples, offering a clear advantage over baselines that use the same LDA identifier but fail to exploit this additional information (Figure 3).

2. *Bridging CNN and VLM-Based TTA Insights*: ROSITA integrates key insights from CNN-based TTA methods such as normalization layer updates with vision-language models (VLMs) (Section 4). While simple in hindsight, this baseline was overlooked in prior VLM-based TTA works Shu et al. (2022); Karmanov et al. (2024); Zhang et al. (2024). In this work, we attempt to highlight how these learnings can translate effectively to VLMs, underscoring their utility as a foundational approach for TTA.

3. *Holistic Design for Open-set TTA*: ROSITA introduces the ReDUCe loss to distinctly separate desired (C_d) and undesired (C_u) class samples using compact feature banks. Although it is inspired by contrastive learning frameworks Chen et al. (2020; 2022), it is specifically designed for open-set TTA: (i) Reliable samples from C_u use nearest C_u samples as negatives, and vice versa (ii) Unlike the C_d+1-way classification in Li et al. (2023), ROSITA forces C_d features to form distinct clusters and pushes C_u features away. (iii) The feature banks are populated only with reliable samples, ensuring robust updates during adaptation. This approach addresses the significant overlap of zero-shot scores s_t between C_d and C_u in vision-language models, reducing misclassification and boosting discriminability.

9) What are the limitations of ROSITA which can be addressed in future?

Although ROSITA performs better than the baselines, if the undesired classes are similar to the desired ones (like CIFAR-10C and CIFAR-100C), the FPR is still quite high, indicating that there is still significant scope for improvement. While in this work, we aim to identify the undesired class samples as "I don't know", in many practical applications these new classes can be of interest and need to be included in the desired classes. This incremental nature of TTA, where the set of desired classes keep growing, can be potentially explored in the future. Additional parameter choices such as adapters, LoRA can be explored for fine-tuning the model.

Appendix. In addition to the analysis presented here, we perform more detailed experimental analysis which we present in the Appendix: C.1 Analysis on error bars, C.2 Analysis of parameter K, C.3 Detailed analysis of ReDUCe Loss components, C.4 Comparison of different C_d vs C_u Class identifiers for Open-set TTA, C.5 Extensive analysis on parameter choice for continuous adaptation of VLMs, D.1 Performance of ROSITA on large Vision Language backbones.

7 Conclusion

In this work, we address the challenging and underexplored problem of **Open-set Single Image Test Time Adaptation** (OSTTA), where models must adapt continuously to shifting data distributions and distinguish between known and unknown classes, all while processing test samples one at a time. To advance research in this area, we establish a comprehensive benchmark for OSTTA using Vision-Language Models (VLMs), bridging the gap between open-set recognition and sequential adaptation in dynamic environments. We propose **ROSITA**, a novel framework specifically designed for OSTTA, overcoming the limitations of prior methods that assume closed-set conditions or batch-wise test processing. ROSITA leverages two dynamically updated feature banks to differentiate between desired and unfamiliar samples. At its core, the ReDUCe loss facilitates effective model adaptation by emphasizing reliable samples while mitigating the negative influence of undesired inputs. Extensive experiments across diverse domain adaptation benchmarks demonstrate that ROSITA consistently outperforms both training-free and prompt-tuning baselines, achieving good accuracy with computational efficiency.

References

Dian Chen, Dequan Wang, Trevor Darrell, and Sayna Ebrahimi. Contrastive test-time adaptation. In *CVPR*, 2022.

Ting Chen, Simon Kornblith, Mohammad Norouzi, and Geoffrey Hinton. A simple framework for contrastive learning of visual representations. In *ICML*, 2020.

Mehdi Cherti, Romain Beaumont, Ross Wightman, Mitchell Wortsman, Gabriel Ilharco, Cade Gordon, Christoph Schuhmann, Ludwig Schmidt, and Jenia Jitsev. Reproducible scaling laws for contrastive language-image learning. In *Proceedings of the IEEE/CVF Conference on Computer Vision and Pattern Recognition*, pp. 2818–2829, 2023.

J. Deng, W. Dong, R. Socher, L. J. Li, K. Li, and L. Fei-Fei. Imagenet: A large-scale hierarchical image database. In *CVPR*, 2009.

Mario Döbler, Robert A Marsden, and Bin Yang. Robust mean teacher for continual and gradual test-time adaptation. In *CVPR*, 2023.

Debidatta Dwibedi, Yusuf Aytar, Jonathan Tompson, Pierre Sermanet, and Andrew Zisserman. With a little help from my friends: Nearest-neighbor contrastive learning of visual representations. In *ICCV*, 2021.

Mark Everingham, Luc Gool, Christopher K. Williams, John Winn, and Andrew Zisserman. The pascal visual object classes (voc) challenge. *IJCV*, 2010.

Ronald A Fisher. The use of multiple measurements in taxonomic problems. *Annals of eugenics*, 7(2):179–188, 1936.

Zhengqing Gao, Xu-Yao Zhang, and Cheng-Lin Liu. Unified entropy optimization for open-set test-time adaptation. In *Proceedings of the IEEE/CVF Conference on Computer Vision and Pattern Recognition*, pp. 23975–23984, 2024.

Kaiming He, Georgia Gkioxari, Piotr Dollár, and Ross Girshick. Mask R-CNN. In *ICCV*, 2017.

Kaiming He, Haoqi Fan, Yuxin Wu, Saining Xie, and Ross Girshick. Momentum contrast for unsupervised visual representation learning. In *CVPR*, 2020.

Dan Hendrycks and Thomas Dietterich. Benchmarking neural network robustness to common corruptions and perturbations. *arXiv preprint arXiv:1903.12261*, 2019.

Dan Hendrycks, Steven Basart, Norman Mu, Saurav Kadavath, Frank Wang, Evan Dorundo, Rahul Desai, Tyler Zhu, Samyak Parajuli, Mike Guo, et al. The many faces of robustness: A critical analysis of out1-of-distribution generalization. In *CVPR*, 2021.

Adilbek Karmanov, Dayan Guan, Shijian Lu, Abdulmotaleb El Saddik, and Eric Xing. Efficient test-time adaptation of vision-language models. In *Proceedings of the IEEE/CVF Conference on Computer Vision and Pattern Recognition*, pp. 14162–14171, 2024.

Muhammad Uzair Khattak, Hanoona Rasheed, Muhammad Maaz, Salman Khan, and Fahad Shahbaz Khan. Maple: Multi-modal prompt learning. In *CVPR*, 2023.

Prannay Khosla, Piotr Teterwak, Chen Wang, Aaron Sarna, Yonglong Tian, Phillip Isola, Aaron Maschinot, Ce Liu, and Dilip Krishnan. Supervised contrastive learning. In *NeurIPS*, 2020.

Ya Le and Xuan Yang. Tiny imagenet visual recognition challenge. *CS 231N*, 7(7):3, 2015.

Yann LeCun, Léon Bottou, Yoshua Bengio, and Patrick Haffner. Gradient-based learning applied to document recognition. *Proceedings of the IEEE*, 86(11):2278–2324, 1998.

Jungsoo Lee, Debasmit Das, Jaegul Choo, and Sungha Choi. Towards open-set test-time adaptation utilizing the wisdom of crowds in entropy minimization. In *ICCV*, 2023.

Yushu Li, Xun Xu, Yongyi Su, and Kui Jia. On the robustness of open-world test-time training: Self-training with dynamic prototype expansion. In *ICCV*, 2023.

Jian Liang, Dapeng Hu, and Jiashi Feng. Do we really need to access the source data? source hypothesis transfer for unsupervised domain adaptation. In *ICML*, 2020.

Yuval Netzer, Tao Wang, Adam Coates, Alessandro Bissacco, Baolin Wu, Andrew Y Ng, et al. Reading digits in natural images with unsupervised feature learning. In *NIPS workshop on deep learning and unsupervised feature learning*, volume 2011, pp. 7. Granada, Spain, 2011.

Shuaicheng Niu, Jiaxiang Wu, Yifan Zhang, Yaofo Chen, Shijian Zheng, Peilin Zhao, and Mingkui Tan. Efficient test-time model adaptation without forgetting. In *ICML*, 2022.

Xingchao Peng, Ben Usman, Neela Kaushik, Judy Hoffman, Dequan Wang, and Kate Saenko. Visda: The visual domain adaptation challenge. *arXiv preprint arXiv:1710.06924*, 2017.

Xingchao Peng, Qinxun Bai, Xide Xia, Zijun Huang, Kate Saenko, and Bo Wang. Moment matching for multi-source domain adaptation. In *ICCV*, pp. 1406–1415, 2019a.

Xingchao Peng, Qinxun Bai, Xide Xia, Zijun Huang, Kate Saenko, and Bo Wang. Moment matching for multi-source domain adaptation. In *ICCV*, 2019b.

Alec Radford, Jong Wook Kim, Chris Hallacy, Aditya Ramesh, Gabriel Goh, Sandhini Agarwal, Girish Sastry, Amanda Askell, Pamela Mishkin, Jack Clark, et al. Learning transferable visual models from natural language supervision. In *ICML*. PMLR, 2021.

Shaoqing Ren, Kaiming He, Ross Girshick, and Jian Sun. Faster r-cnn: Towards real-time object detection with region proposal networks. In *NeurIPS*, 2015.

Jameel Hassan Abdul Samadh, Hanan Gani, Noor Hazim Hussein, Muhammad Uzair Khattak, Muzammal Naseer, Fahad Khan, and Salman Khan. Align your prompts: Test-time prompting with distribution alignment for zero-shot generalization. In *NeurIPS*, 2023.

Steffen Schneider, Evgenia Rusak, Luisa Eck, Oliver Bringmann, Wieland Brendel, and Matthias Bethge. Improving robustness against common corruptions by covariate shift adaptation. In *NeurIPS*, 2020.

Manli Shu, Weili Nie, De-An Huang, Zhiding Yu, Tom Goldstein, Anima Anandkumar, and Chaowei Xiao. Test-time prompt tuning for zero-shot generalization in vision-language models. In *NeurIPS*, 2022.

Dequan Wang, Evan Shelhamer, Shaoteng Liu, Bruno Olshausen, and Trevor Darrell. Tent: Fully test-time adaptation by entropy minimization. In *ICLR*, 2021.

Hualiang Wang, Yi Li, Huifeng Yao, and Xiaomeng Li. Clipn for zero-shot ood detection: Teaching clip to say no. In *ICCV*, 2023.

Ce Zhang, Simon Stepputtis, Katia P Sycara, and Yaqi Xie. Dual prototype evolving for test-time generalization of vision-language models. In *NeurIPS*, 2024.

Bingchen Zhao, Haoqin Tu, Chen Wei, Jieru Mei, and Cihang Xie. Tuning layernorm in attention: Towards efficient multi-modal llm finetuning. *arXiv preprint arXiv:2312.11420*, 2023.

APPENDIX

A Gradient Analysis of the ReDUCe Loss

Here, we delve deeper into the ReDUCe loss function in ROSITA, breaking down its key components and mathematically demonstrate why the proposed objective improves the separation of C_d and C_u samples. We'll focus on contrastive loss components L_D and L_U which are designed to improve discriminability.

ReDUCe loss in a nutshell. A test sample x_t arrives at time t with feature representation f_t. Two feature banks, $\mathcal{M}_w$ and $\mathcal{M}_s$ store reliable sample features from C_d and C_u respectively. ReDUCe loss aims to pull the test sample's feature f_t towards its positive samples z^+, which are its K nearest neighbors $Q^d = \mathrm{k}NN(f_t; M_d)$ if it is a reliable C_d sample or $Q^u = \mathrm{k}NN(f_t; M_u)$ if it is a reliable C_u sample. The feature f_t is pushed away from its negative samples z^-, which are the K nearest neighbors from the undesired feature bank M_u if it is a reliable C_d sample or from the desired feature bank M_d if it is a reliable C_u sample. The features f_t, z^+, z^- are all unit norm vectors. The key to understanding the behavior of the proposed loss is to analyze its gradient.

Gradient of L_D with respect to f_t:

The contrastive loss for desired class samples L_D is defined as:

$$\begin{aligned}\mathcal{L}_D &= -\frac{1}{K^+}\sum_{z^+\in Q^d}\mathbf{1}(y^+=\hat{y}_t)\log\frac{\exp\left(\mathrm{sim}\left(f_t,z^+\right)/\tau\right)}{\sum_{z^-\in Q^u}\exp(\mathrm{sim}(f_t,z^-)/\tau)}\\ \frac{\partial\mathcal{L}_D}{\partial f_t} &= -\frac{1}{K^+}\sum_{z^+\in Q^d}\mathbf{1}(y^+=\hat{y}_t)\frac{\partial}{\partial f_t}\log\frac{\exp\left(\mathrm{sim}\left(f_t,z^+\right)/\tau\right)}{\sum_{z^-\in Q^u}\exp(\mathrm{sim}(f_t,z^-)/\tau)}\end{aligned} \tag{11}$$

The loss is of the log-softmax structure. Consider gradient of the following term:

$$\frac{\partial}{\partial f_t}\log\frac{\exp\left(\mathrm{sim}\left(f_t,z^+\right)/\tau\right)}{\sum\limits_{z^-\in Q}\exp(\mathrm{sim}(f_t,z^-)/\tau)} = \frac{\partial}{\partial f_t}\left(\frac{\mathrm{sim}\left(f_t,z^+\right)}{\tau}\right) - \frac{\partial}{\partial f_t}\log\sum_{z^-\in Q}\exp(\mathrm{sim}(f_t,z^-)/\tau)$$

The gradients of the two terms involved are

$$\begin{aligned}\frac{\partial}{\partial f_t}\left(\frac{\mathrm{sim}\left(f_t,z^+\right)}{\tau}\right) &= \frac{z^+}{\tau}\\ \frac{\partial}{\partial f_t}\log\sum_{z^-\in Q}\exp(\mathrm{sim}(f_t,z^-)/\tau) &= \frac{\sum\limits_{z^-\in Q}\frac{\partial}{\partial f_t}\exp(\mathrm{sim}(f_t,z^-)/\tau)}{\sum\limits_{z^-\in Q}\exp(\mathrm{sim}(f_t,z^-)/\tau)}\\ &= \frac{1}{\tau}.\frac{\sum\limits_{z^-\in Q}\exp(\mathrm{sim}(f_t,z^-)/\tau)}{\sum\limits_{z^-\in Q}\exp(\mathrm{sim}(f_t,z^-)/\tau)z^-}\\ &= \frac{1}{\tau}.\sum_{z^-\in Q}p(z^-)z^-\end{aligned} \tag{12}$$

The final gradient of the log-softmax term is

$$\frac{\partial}{\partial f_t}\log\frac{\exp\left(\mathrm{sim}\left(f_t,z^+\right)/\tau\right)}{\sum\limits_{z^-\in Q}\exp(\mathrm{sim}(f_t,z^-)/\tau)} = \left(z^+ - \sum_{z^-\in Q}p\left(z^-\right)z^-\right)$$

where $p\left(z^-\right)$is the softmax probability of the negative samples defined as

$$p\left(z^{-}\right)=\frac{\exp\left(\operatorname{sim}\left(f_t, z^{-}\right)/\tau\right)}{\sum\limits_{z' \in Q^{-}} \exp\left(\operatorname{sim}\left(f_t, z'\right)/\tau\right)}$$

Substituting Equation 12 in Equation 11, we get the gradient of the desired sample contrastive loss L_D with respect to f_t as

$$\frac{\partial \mathcal{L}_D}{\partial f_t}=-\frac{1}{K^{+}} \sum_{z^{+} \in Q^{d}} \mathbf{1}(y^{+}=\hat{y}_t)\left(z^{+}-\sum_{z^{-} \in Q^{u}} p\left(z^{-}\right) z^{-}\right) \tag{13}$$

Gradient of L_D with respect to f_t:

The contrastive loss for desired class samples L_D is defined as:

$$\begin{aligned}\mathcal{L}_U &= -\frac{1}{K} \sum_{z^{+} \in Q^{u}} \log \frac{\exp\left(\operatorname{sim}\left(f_t, z^{+}\right)/\tau\right)}{\sum\limits_{z^{-} \in Q^{d}} \exp(\operatorname{sim}(f_t, z^{-})/\tau)} \\ \frac{\partial \mathcal{L}_U}{\partial f_t} &= -\frac{1}{K^{+}} \sum_{z^{+} \in Q^{u}} \frac{\partial}{\partial f_t} \log \frac{\exp\left(\operatorname{sim}\left(f_t, z^{+}\right)/\tau\right)}{\sum\limits_{z^{-} \in Q^{d}} \exp(\operatorname{sim}(f_t, z^{-})/\tau)}\end{aligned} \tag{14}$$

Substituting Equation 12 in Equation 14, we get:

$$\frac{\partial \mathcal{L}_U}{\partial f_t}=-\frac{1}{K^{+}} \sum_{z^{+} \in Q^{u}}\left(z^{+}-\sum_{z^{-} \in Q^{d}} p\left(z^{-}\right) z^{-}\right) \tag{15}$$

Interpretation of the Gradients:

- Both the gradient terms in Equations 13 and 15 have two components: Positive term z^{+} and Negative term $p\left(z^{-}\right) z^{-}$. The positives and negatives are suitably chosen from the desired and undesired feature banks.
- Positive term z^{+}: The term z^{+}pulls the test feature f_t closer to its feature vectors z^{+}. This term represents the attraction force that encourages C_d samples to cluster together in L_D and C_u samples to cluster together in L_U.
- Negative term $p\left(z^{-}\right) z^{-}$: The negative samples z^{-} exert a repulsive force, pushing f_t away from them. The strength of this repulsion is controlled by the softmax probabilities $p\left(z^{-}\right)$, where higher similarity between f_t and z^{-}increases the repulsion force. This inherently models the degree of hard negatives from the negative feature bank.
- The overall gradient update encourages f_t to move closer to its positives while moving away from its negatives, enhancing the separation between samples from C_d and C_u classes.

B Baselines

B.1 Vision Language Models

CLIP Radford et al. (2021) is a multimodal VLM consisting of two modules: Vision encoder and Text encoder denoted as $\mathcal{F}_V$ and $\mathcal{F}_T$ respectively. During pre-training, the two modules are jointly trained in a contrastive self-supervised fashion to align massive amounts of web scrapped image-text pairs. CLIP has demonstrated impressive zero-shot performance across a wide variety of datasets.

MaPLe Khattak et al. (2023) is a multimodal prompt learner model that simultaneously adapts both vision and text encoders while fine-tuning CLIP for downstream tasks. They use learnable text prompts $\boldsymbol{p}_T$ and bridge the two modalities using visual prompts obtained as $\boldsymbol{p}_V = \text{Proj}(\boldsymbol{p}_T)$. Learnable tokens are also introduced in the deeper layers of both image and text encoders, to enable progressive adaptation of the features.

B.2 Methods

ZSEval (Radford et al., 2021): Given a test image x_t, the image feature is extracted from the vision encoder as $f_t = \mathcal{F}_V(x_t)$. For a C-class classification problem, the classifier is obtained by prepending a predefined text prompt $\boldsymbol{p}_T$="A photo of a", with the class names $\{c_1, c_2, \dots c_C\}$ to form class specific text inputs $\{\boldsymbol{p}_T, c_i\}$ for $i \in \{1, \dots C\}$. These texts are then embedded through the text encoder as $\boldsymbol{t}_i = \mathcal{F}_T(\{\boldsymbol{p}_T; c_i\})$ to get the text classifiers $\{\boldsymbol{t}_1, \boldsymbol{t}_2, \dots \boldsymbol{t}_C\}$. The class prediction is made by identifying the text feature $\boldsymbol{t}_i$ which has the highest similarity with the image feature f_t.

TPT Shu et al. (2022) aims to improve the zero shot generalization ability of CLIP by providing custom adaptable context for each image. This is done by prepending learnable text prompts $\boldsymbol{p}_T$ to the class names instead of a predefined text prompt. The text classifiers $\boldsymbol{t}_i = \mathcal{F}_T(\{\boldsymbol{p}_T; c_i\}), i \in \{1, 2, \dots C\}$ are now a function of these learnable prompts, which are specially adapted for each test image using an entropy minimization objective as $\arg\min_{\boldsymbol{p}_T} \mathcal{L}_{\text{ent}}$. The entropy is obtained using the average score vector of the filtered augmented views.

PromptAlign (PAlign) (Samadh et al., 2023) leverages multimodal prompt learner model MaPLe Khattak et al. (2023) to facilitate the adaptation of both vision and language encoders for each test sample. They align the token distributions of source and target domains, considering ImageNet as a proxy for the source dataset of CLIP. The vision and language prompts of MaPLe are optimized with the objective $\arg\min_{\{\boldsymbol{p}_V, \boldsymbol{p}_T\}} \mathcal{L}_{ent} + \mathcal{L}_{align}$ for each sample x_t.

TPT-C Shu et al. (2022)/PAlign-C (Samadh et al., 2023): We adapt TPT and PAlign for continuous model update, which we refer as TPT-C and PAlign-C respectively. The prompts $\{\boldsymbol{p}_T\}$ and $\{\boldsymbol{p}_V, \boldsymbol{p}_T\}$ in TPT and PAlign are continuously updated with the test stream with their respective test objectives.

(K+1)PC (Li et al., 2023): This was the first work exploring open world TTA, however it was done in the context of CNNs and not VLMs. Also, the test samples come in batches, while we perform single image TTA. We adapt this method for our problem setting as follows: As we use VLMs, we use the text prototypes (instead of the source prototypes). The prototype pool is dynamically updated by adding features of reliable test samples recognized to belong to undesired classes. The vision encoder is updated using a (K+1) way prototypical cross entropy loss.

TDA (Karmanov et al., 2024): TDA is a training-free dynamic adapter for test-time adaptation in vision-language models, utilizing a lightweight key-value cache for efficient pseudo label refinement without backpropagation.

DPE (Zhang et al., 2024):DPE accumulates task-specific knowledge by dynamically evolving two sets of prototypes, textual and visual, during test time. These prototypes are refined to capture increasingly accurate multi-modal representations for target classes. To ensure consistency between modalities, DPE incorporates learnable residuals for each test sample, aligning textual and visual prototypes for improved representation alignment.

UniEnt Gao et al. (2024): This is a very recent work addressing open-set TTA in the context of CNNs. They use a Distribution Aware Filter (DAF) based on Gaussian Mixture Modeling of the scores to distinguish between desired and undesired class samples. They employ entropy minimization and entropy maximization objectives for desired and undesired class samples respectively.

We equip all the baselines with the same LDA based Desired vs Undesired class identifier described in Section 2.2 for fair comparison of the TTA methods for this problem.

B.3 Datasets

We experiment with a diverse set of datasets, encompassing corruption datasets, style transfer datasets, and other common datasets.

CIFAR10-C Hendrycks & Dietterich (2019) is a small-scale corruption dataset of 10 classes with 15 common corruption types. It consists of 10,000 images for each corruption.

CIFAR-100C Hendrycks & Dietterich (2019) is also a corruption dataset with 100 classes and 15 corruption types. It also consists of 10,000 images for each corruption.

ImageNet-C Hendrycks & Dietterich (2019) is a large-scale corruption dataset spanning 1000 categories with a total of 50,000 images. 15 types of corruption images are synthesized from these 50,000 images.

ImageNet-R Hendrycks et al. (2021) is a realistic style transfer dataset encompassing interpretations of 200 ImageNet classes, amounting to a total of 30,000 images.

VisDA Peng et al. (2017) is a synthetic-to-real large-scale dataset, comprising of 152,397 synthetic training images and 55,388 real testing images across 12 categories.

DomainNet Peng et al. (2019a) is a large-scale domain adaptation dataset. We use the Clipart, Painting and Sketch domains with 345 categories from the DomainNet dataset for our experiments.

MNIST LeCun et al. (1998) is a dataset of handwritten images consisting of 60,000 training and 10,000 testing images.

SVHN Netzer et al. (2011) is also a digits dataset with house numbers captured from real streets. It consists of 50,000 training images and 10,000 testing images.

We perform experiments on eight domains D_d for desired class samples. The corresponding D_u are chosen such that there is no overlap between the classes C_d and C_u as described in Table 8. The 15 corruptions of CIFAR-10C/100C and ImageNet-C fall into four categories: synthetic weather effects, per-pixel noise, blurring, and digital transforms. *snow* corruption is a synthesized weather effect on which all the main experiments of CIFAR-10C, CIFAR-100C and ImageNet-C are done. To evaluate the robustness of our method across different corruption types, we do additional experiments with *impulse noise* , *motion blur* and *jpeg compression* corruptions from the categories per-pixel noise, blurring and digital transforms respectively and report the results in Section D.2.

Table 8: Details of desired and undesired class dataset combinations

Datasets		# images		
D_d	D_u	D_d	D_u	Total
CIFAR-10C	MNIST, SVHN, Tiny ImageNet, CIFAR-100C	10000	10000	20000
CIFAR-100C	MNIST, SVHN, Tiny ImageNet, CIFAR-10C	10000	10000	20000
ImageNet-C	MNIST, SVHN	50000	50000	100000
ImageNet-R	MNIST, SVHN	30000	30000	60000
VisDA	MNIST, SVHN	50000	50000	100000
Clipart	MNIST, SVHN	29208	29208	58416
Painting	MNIST, SVHN	43700	43700	87400
Sketch	MNIST, SVHN	41832	41832	83664

B.4 Implementation Details

Here, we describe the parameters chosen for all the baseline methods and our proposed method.

TPT Shu et al. (2022): The prompt is initialized with the default *A photo of a* text. The corresponding 4 tokens in the input text embedding space are optimized for each test image. The prompt is **reset** after each update. A single test image is augmented 63 times using random resized crops to create a batch of 64 images. The confident samples with 10% lowest entropy are selected. The test time loss is the entropy of the averaged prediction of the selected confident samples. AdamW optimizer with a learning rate of $5e^{-4}$ is used, following Shu et al. (2022).

PAlign Samadh et al. (2023): Following PromptAlign Samadh et al. (2023), MaPLe Khattak et al. (2023) model trained on ImageNet using 16-shot training data with 2 prompt tokens for a depth of 3 layers is used. The prompts on both the text and vision encoders are optimized on a single test image. Similar to TPT, 10% of 64 augmentations are selected to compute the entropy loss. The token distribution loss to align the token statistics of test with that of source data is computed for all 64 images. AdamW optimizer with a learning rate of $5e^{-4}$ to update the prompts for each image, following Samadh et al. (2023). The prompts are **reset** to the ImageNet trained prompts after each update.

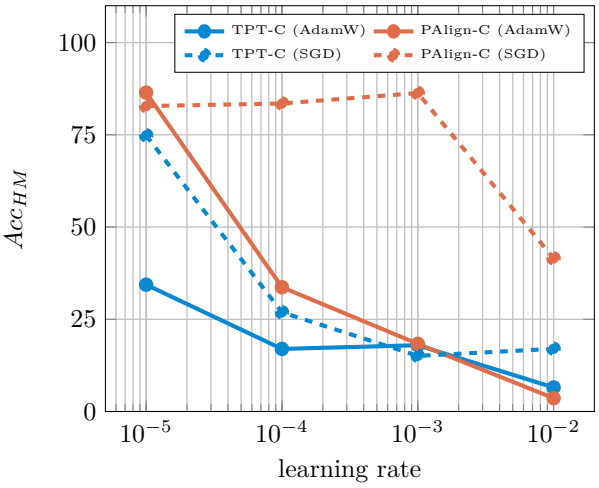

Figure 5: Performance of TPT-C and PAlign-C for CIFAR-10C/MNIST with AdamW and SGD optimizer on varying learning rates.

TPT-C Shu et al. (2022)/ PAlign-C Samadh et al. (2023): We create the continuous prompt update versions of TPT and PAlign as TPT-C and PAlign-C respectively. The only difference is that the prompts are continuously updated using the test stream of samples. If a sample is detected as reliable C_d sample, the respective test time objectives are used to update the prompts. For this purpose, we vary the learning rate and optimizer to select the best optimizer for continuous prompt update. On performing experiments on CIFAR-10C/MNIST data, from Figure 5 we observe that SGD optimizer with learning rate 10^{-5} works the best for continuous prompt update and hence we use this for all the experiments of TPT-C and PAlign-C.

(K+1)PC Li et al. (2023): The vision encoder is updated using a (K+1) way prototypical cross entropy loss . The prototypes are updated using the test stream of samples. The learning rate is set to 0.001.

TDA (Karmanov et al., 2024): We use τ_t from the LDA based C_d vs C_u identifier to recognise the desired and undesired class samples. Following Karmanov et al. (2024), we set the shot capacity to 3 and the number of key-value caches is C_d as we use the adapter only for desired class samples.

DPE (Zhang et al., 2024): We use the same LDA based C_d vs C_u identifier to recognise the desired and undesired class samples. We use the same hyperparameters presented in Zhang et al. (2024). A priority queue storing 3 visual features per class is used. The text and visual prototype residuals are updated with a learning rate of 0.0006 using AdamW optimizer.

UniEnt Gao et al. (2024): We use the UniEnt objective in combination with LDA based class indentifier. The entropy minimization and maximization objectives are used for desired and undesired class samples respectively. The LayerNorm parameters are updated with a learning rate of 0.001 using SGD optimizer.

ROSITA: We use SGD optimizer with a learning rate of 0.001 to update the LayerNorm affine parameters of the Vision encoder. We set the size of score bank $\mathcal{S}$ to 512, number of neighbours K to 5 and the size of M_u is set to to 64.

C Additional Analysis

In this section, in addition to the analysis done in Section 6, we study the robustness of the proposed method ROSITA more extensively, in the terms of (1) Error bars on different test data streams, (2) Role of the parameter K, the number of neighbours, (3) Analysis of the scores s_t on using different combinations of the proposed loss components, (4) Comparison of different C_d vs C_u Class identifiers for Open-set TTA.

C.1 Analysis on error bars

To study the robustness of our method for differently ordered test streams, we run ROSITA with five random seeds and report the Mean and Standard deviation of the Acc_{HM} in Table 9 for CIFAR-10C/100C as D_d and MNIST, SVHN, Tiny ImageNet, CIFAR-100C/10C as D_u (corresponding to our results in Table 3 in the main paper). We observe that the variance in the performance of ROSITA is very low, reinforcing the robustness of the proposed method for different shuffled datasets and augmentations created.

Table 9: Performance (Mean and Standard deviation of Acc_{HM}) of ROSITA across 5 random seeds for CIFAR-10/100C as D_d with 4 other datasets as D_u.

$D_d \backslash D_u$	MNIST	SVHN	Tiny	CIFAR-100/10C
CIFAR-10C	84.07 ± 0.023	78.90 ± 0.038	80.10 ± 0.014	69.44 ± 0.018
CIFAR-100C	57.09 ± 0.041	47.90 ± 0.047	55.95 ± 0.051	48.10 ± 0.024

C.2 Analysis on parameter K

Table 10: Performance (Acc_{HM}) on varying K with MNIST as D_u.

D_d	$\lvert C_d \rvert$	K					
		0	1	3	5	7	9
CIFAR-10C	10	80.97	83.9	84.32	84.17	84.10	84.02
ImageNet-R	200	64.32	83.65	83.87	83.53	83.39	83.42
ImageNet-C	1000	42.05	48.35	47.17	48.53	48.37	47.73

We vary the hyperparameter K which represents the number of positives and negatives chosen in Equation 6 and 7 and report the results (Acc_{HM}) in Table 10. The size of the feature bank $\mathcal{M}_d$ is set as $N_d = K \times C_d$. N_d increases with the number of classes as well as the number of neighbours K. We set K to be 5 in all main results reported, which corresponds to feature bank size N_d of 50, 1000, 5000 respectively for the datasets CIFAR-10C, ImageNet-R and ImageNet-C respectively. In Table 10, we use the notation $K = 0$ to correspond to the case where only the reliable pseudo label loss $\mathcal{L}_{Re}$ is used. The results show that even with $K = 1$, there is a significant improvement in Acc_{HM} when compared to the case where $\mathcal{L}_D, \mathcal{L}_U$ is not used ($K = 0$). On further increasing K, we observe improvement only for the CIFAR-10C as D_d, but the performance is similar for ImageNet-R and ImageNet-C for higher values of K as well. Further, we investigate this observation that the performance of ROSITA is similar on significantly varying K or the feature bank size. For $K = 5$, we check the average number of positives actually selected for L_D in Equation 6 for each of these datasets. We find this to be $4.1, 2.5$ and 1.5 for CIFAR-10C, ImageNet-R and ImageNet-C respectively. This agrees with the results in Table 10 where K of 3, 5 works better compared to 1 as more neighbours have common pseudo label, aiding the clustering of classes of interest. For CIFAR-10C and ImageNet-R, using $K < 5$ suffices and for ImageNet-C as only 1-2 neighbours are matched for majority of reliable desired class samples, setting $K = 1$ suffices. For practical purposes, this observation suggests that the buffer size for M_d can indeed be reduced based on storage budget available depending on the application and device the model is deployed on. For e.g., if the memory budget available can store only upto 1000 features, K can be set flexibly depending on the number of classes of interest. For ImageNet-C with 1000 classes, K can be set to 1.

C.3 Detailed analysis of ReDUCe Loss components

We provide detailed results of Table 4 including all the five metrics in Table 11. Additionally, we visualise the histograms of the scores s_t on using different combinations of the loss components of ReDUCe Loss in the Figures 6, 7, justifying their role in better discrimination of samples from C_d and C_u.

Table 11: Detailed performance metrics analysing the ReDUCE Loss components.

$\mathcal{L}_{Re}$	$\mathcal{L}_D$	$\mathcal{L}_U$	CIFAR-10C/MNIST					ImageNet-R/MNIST				
			AUC	FPR	Acc_D	Acc_U	Acc_{HM}	AUC	FPR	Acc_D	Acc_U	Acc_{HM}
✗	✗	✗	91.91	85.04	60.82	99.77	75.57	91.27	91.09	55.67	99.90	71.50
✓	✗	✗	95.29	30.82	68.36	99.30	80.97	81.07	99.02	48.42	95.76	64.32
✗	✓	✗	95.23	28.91	66.93	98.52	79.71	87.73	94.67	51.13	98.34	67.28
✗	✗	✓	98.61	12.73	66.60	99.68	79.84	99.39	4.81	67.81	99.99	80.82
✗	✓	✓	99.27	4.15	67.76	99.73	80.69	99.48	4.40	69.38	99.98	81.92
✓	✓	✓	99.10	7.63	72.81	99.74	84.17	99.44	4.29	71.73	99.98	83.53

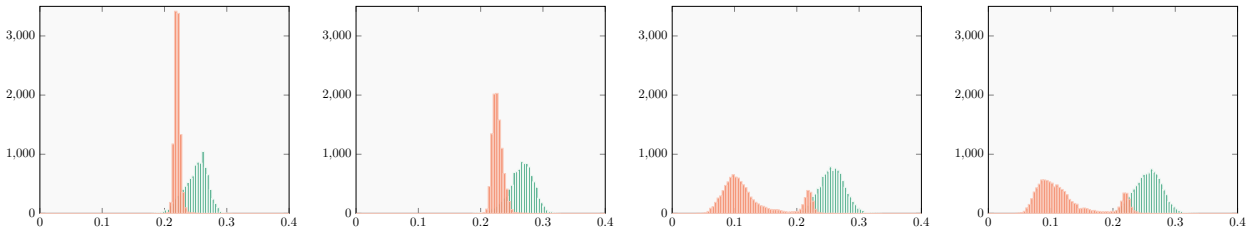

(a) ZSEval (b) L_{Re} (c) $L_D + L_U$ (d) $L_{Re} + L_D + L_U$

Figure 6: Histograms of C_d and C_u class scores for ZS-Eval and on using different loss components of the proposed ReDUCe loss on CIFAR-10C/MNIST dataset with CLIP.

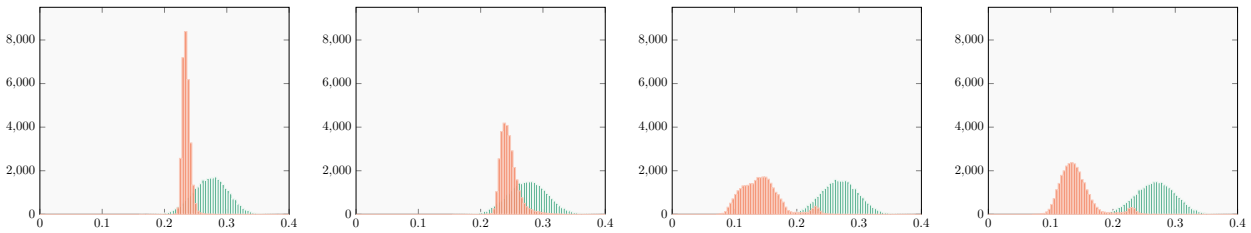

(a) ZSEval (b) L_{Re} (c) $L_D + L_U$ (d) $L_{Re} + L_D + L_U$

Figure 7: Histograms of C_d and C_u class scores for ZS-Eval and on using different loss components of the proposed ReDUCe loss on ImageNet-R/MNIST dataset with CLIP.

From Figure 6 and 7, we observe that, on using just $\mathcal{L}_{Re}$, the scores of C_d and C_u classes still sufficiently overlap, similar to the case of ZSEval. The performance purely depends on the quality of pseudo labels of the detected reliable desired class samples. In CIFAR-10C, as there are only 10 classes and given that the performance of ZSEval in CIFAR-10C is fairly good, it ensures good quality pseudo-labels, hence resulting in overall better metrics even using $\mathcal{L}_{Re}$ as shown in Table 11. ImageNet-R dataset inherently has more confusion as it is a 200-way classification problem. This naturally could result in lower quality pseudo-labels, in turn degrading the performance compared to ZSEval. In addition, using $\mathcal{L}_{Re}$ for desired class samples that are misclassified as undesired class samples increases the FPR and results in a decrease in overall metrics compared to ZSEval. However, using $\mathcal{L}_D$ and $\mathcal{L}_U$ separates the scores s_t of the samples from C_d and C_u, resulting in two distinct peaks as seen in Figure 6 and 7, which in turn results in a significantly low FPR as reported in Table 11. Hence, the best results (Table 11) are obtained using the proposed ReDUCe loss, where

all the loss components help each other to better discriminate the desired classes C_d from C_u (measured by AUC, FPR) and also improving the C_d-way accuracy (Acc_D) on desired classes.

C.4 Comparison of different C_d vs C_u Class identifiers for Open-set TTA

To study the role of the C_d vs C_u class identifiers in Open-set Single Image TTA, we experiment with three class identifiers, on five datasets as D_d with MNIST as D_u using CLIP backbone.

(1) Simple thresholding based on Maximum Softmax Probability(MSP): We set fixed thresholds τ_u, τ_d to identify reliable samples from C_d and C_u classes respectively and τ_t to distinguish between C_d and C_u samples. We combine this class identifier with the ReDUCe loss of the proposed ROSITA framework.

(2) Distribution Aware Filter (DAF) Gao et al. (2024) : We adopt the Distribution Aware Filter proposed in UniEnt Gao et al. (2024), a very recent method on open-set TTA using CNNs, where they model the scores s_t (similarity between image feature and source prototype) as a Gaussian Mixture Model for each batch. In our case, as we do single image TTA, we use a score bank as described in Section 2.2 as a proxy for the batch of samples, to estimate the parameters of the GMM. As it is a 2-component GMM, we identify a sample as a desired class sample if the probability $\pi(x_t)$ of the sample belonging to the desired classes(component with higher mean estimated) is greater than 0.5 or vice versa. The GMM based class identifier is defined as follows:

$$\hat{y} \begin{cases} \in C_d & \text{if } \pi(x_t) \geq 0.5 \\ \in C_u & \text{if } \pi(x_t) < 0.5 \end{cases} \tag{16}$$

We combine this class identifier with the Unified entropy objective and ReDUCe loss proposed by UniEnt Gao et al. (2024) and our proposed ROSITA framework respectively.

(2) Linear Discriminant Analysis (LDA) based Li et al. (2023) : As described in Section 2.2, we set τ_d to μ_d and τ_u to μ_u to identify reliable C_d and C_u samples to perform TTA. We set τ_t to μ_u to distinguish between C_d and C_u samples. The thresholds are estimated in an online manner using the score bank $\mathcal{S}$. The LDA based class identifier is defined as follows:

$$\hat{y} \begin{cases} \in C_d & \text{if } s_t \geq \tau_t^* \\ \in C_u & \text{if } s_t < \tau_t^* \end{cases} \tag{17}$$

We combine this class identifier with the Unified entropy objective and ReDUCe loss proposed by UniEnt Gao et al. (2024) and our proposed ROSITA framework respectively. The three thresholds for ReDUCe loss in Table 12 correspond to $\tau_u/\tau_t/\tau_d$ where τ_u and τ_d is used to identify reliable test samples and τ_t is used to distinguish between C_d and C_u samples. In the case of DAF with ReDUCe loss, we use the means μ_d^* and μ_* for the two gaussian mixture components to identify reliable samples.

Table 12: Comparison of C_d vs C_u class identifiers: MSP vs DAF vs LDA. The three thresholds for ReDUCe loss correspond to $\tau_u/\tau_t/\tau_d$ where τ_u and τ_d is used to identify reliable test samples and τ_t is used to distinguish between C_d and C_u samples. In the case of DAF with ReDUCe loss, we use the estimated means μ_d^* and μ_u^* of the two Gaussian mixture components to identify reliable samples.

C_d vs C_s	Threshold	Test-time objective	D_u: MNIST				
			C-10C	C-100C	IN-C	IN-R	VisDA
MSP	0.4/0.6/0.8	ReDUCe	43.44	34.42	1.20	77.12	88.49
	0.3/0.5/0.7		33.70	32.60	1.74	80.29	50.87
	0.5/0.5/0.5		22.82	37.41	1.91	30.90	32.31
LDA	$s_t > \tau_t$	UniEnt	75.62	48.31	41.53	71.73	78.09
DAF	$\pi(x_t) > 0.5$		79.43	50.12	46.52	79.30	86.79
LDA	$\mu_u/\tau_t/\mu_d$	ReDUCe	**84.17**	**57.34**	**48.53**	**83.53**	90.64
DAF	$\mu_u^*/0.5/\mu_d^*$		83.56	55.37	48.33	83.32	**90.97**

Our key observations based on the results in Table 12 are as follows:

Fixed vs Dynamic Thresholds: The performance of both, DAF and LDA based class identifier is significantly better than the simple thresholding case on adaptation using ReDUCe loss. The thresholds estimated in an online manner using the score bank $\mathcal{S}$ are more reliable than fixed thresholds. The DAF and LDA-based class identifier is able to better discriminate between C_d and C_u samples, resulting in better performance.

UniEnt vs ReDUCe loss: The performance on using ReDUCe loss (with either DAF or LDA class identifier) is significantly better than using the Unified entropy objective proposed in UniEnt Gao et al. (2024). The ReDUCe loss components aid each other to better discriminate the desired classes C_d from C_u (measured by AUC, FPR) and also improve the C_d-way accuracy (Acc_D) on desired classes.

LDA vs DAF with ReDUCe loss: The performance of LDA and DAF based class identifier perform very similarly when used in combination with ReDUCe loss. This suggests that ReDUCe loss in ROSITA is robust to the choice of a dynamically updating class identifier.

Why is ReDUCe loss better than Unified entropy objective for Open-set TTA of VLMs?

- Both LDA Li et al. (2023) and DAF Gao et al. (2024) were proposed for CNN based open-set TTA where a source model is trained on say clean data and is adapted to new domains, with the observation that the feature-prototype similarity scores s_t can distinguish desired and undesired class samples. In the case of VLMs, the source model is trained on a large scale dataset and is adapted to potentially unseen/corrupted/covariate-shifted data. *The prior that the feature-prototype similarity scores s_t can distinguish desired and undesired class samples does not translate to VLMs as the scores overlap significantly,* as observed in ZSEval histogram plots in Figures 3 6 7.

- In the case of CNNs, where the the initial scores are well separated and model has access to a batch of test samples at a time, UniEnt leverages this to further aid the separation of desired and undesired class samples in the batch through the UniEnt objective. In the case of VLMs, the scores are not well separated initially. This results in the means μ_d and μ_u in the case of LDA to be very close leading to misclassification of C_d and C_u class samples using the estimated threshold τ_t. Similarly, in the case of DAF, the two components of GMM would not be very distinctive to well distinguish desired and undesired class samples. This misclassification can result in entropy minimization being applied on C_u samples and entropy maximization on C_d samples, which is undesirable. Employing UniEnt objective with several misclassified samples may not actually separate desired and undesired classes, as also empirically observed in Tables 1 2 3 (UniEnt has high FPR rate in general). Entropy maximization of C_u samples does not explicitly enforce the separation of desired and undesired class samples in the feature space.

- The L_D and L_U loss components of ReDUCe loss explicitly enforce the separation desired and undesired class samples in the common VL latent space, while the L_{Re} loss aims to only align the desired class samples to align with the text prototypes. With time, the model is adapted such that undesired class samples are away from the desired class samples and also the text prototypes. This ReDUCe loss addresses the challenges in single image open-set TTA in a holistic manner, resulting in better performance.

- On adopting UniEnt objective to single-image TTA, either entropy minimization or maximization loss would be active based on whether a test sample is identified as desired or undesired class sample, which is a limitation, as the objective cannot enforce distinction between the two types of features.

- In the case of CNNs, where the the initial scores are well separated and model has access to a batch of test samples at a time, UniEnt leverages this to further aid the separation of desired and undesired class samples in the batch through the UniEnt objective. In the case of VLMs, the scores are not well separated initially, hence the ReDUCe loss components (with the help of feature banks) acts as the driving force to better separate the desired and undesired class samples in the common latent space, resulting in lower FPR rates as a consequence.

C.5 Extensive analysis on parameter choice for continuous adaptation of VLMs

Our initial experiments showed that updating LayerNorm parameters with simple entropy objective can effectively improve closed-set TTA performance. We illustrate this in Section 4 on CIFAR-10C dataset. Further, to justify our choice of updating LayerNorm parameters, we present the detailed experiments we conducted based on the following choices: (a) **Learnable parameters**: (1) Prompts, (2) Full network, (3) First Attention Block of ViT, (4) Last Attention Block of ViT (5) Prompts+LayerNorm(LN), (6) LayerNorm parameters (Zhao et al., 2023) (b) **Datasets**: In addition to CIFAR-10C (Section 4), we experiment with ImageNet-R, a relatively large scale dataset consisting of 30,000 images from 200 classes. (c) **Optimizer**: Along with SGD, we experiment with AdamW optimizer also used in [1], with varying learning rates on both CIFAR-10C and ImageNet-R dataset. We consistently observe that LayerNorm parameters is in general, a good choice to update the model.

Table 13: Accuracy on updating different parameter groups on CIFAR-10C and ImageNet-R datasets.

Optimizer	Parameters	CIFAR-10C					ImageNet-R				
		$1e^{-6}$	$1e^{-5}$	$1e^{-4}$	$1e^{-3}$	$1e^{-2}$	$1e^{-6}$	$1e^{-5}$	$1e^{-4}$	$1e^{-3}$	$1e^{-2}$
SGD	Prompts	73.40	31.04	12.53	11.18	10.19	73.97	74.17	74.71	25.68	10.63
	Full	10.48	10.44	9.99	10.00	10.01	14.18	7.19	0.65	0.65	0.42
	First Block	75.1	76.12	78.27	13.07	10.01	73.84	74.31	74.91	8.76	0.32
	Last Block	73.45	72.42	59.44	10.17	10.02	75.95	77.93	24.82	0.52	0.67
	Prompts+LN	73.82	46.77	24.71	10.24	10.18	73.76	75.09	76.35	28.72	11.74
	LayerNorm	74.35	76.61	80.41	**84.58**	11.69	74.13	74.35	75.23	**76.92**	33.07
AdamW	Prompts	72.40	18.6	12.83	10.04	10.08	74.4	75.17	27.93	6.82	4.37
	Full	10.32	10.03	10.00	10.00	9.97	14.83	0.95	0.28	0.52	0.66
	First Block	79.05	24.70	10.84	10.00	10.00	74.6	74.8	5.68	0.26	0.15
	Last Block	59.23	10.84	10.49	10.00	10.01	77.44	10.67	0.51	0.25	0.33
	Prompts+LN	75.01	72.10	21.92	13.33	10.01	74.52	76.45	12.99	8.87	5.55
	LayerNorm	76.10	81.57	**85.9**	85.27	10.03	73.96	75.64	78.28	**78.81**	31.47

D Additional Experiments

In addition to the results presented in the main paper, we perform additional experiments supporting the claims made and for more comprehensive understanding of the analysis presented in Section 6.

D.1 Performance of ROSITA on large Vision Language backbones

Here, in addition to CLIP ViT-B/16 Radford et al. (2021) and MAPLE Khattak et al. (2023) backbones, we perform experiments using large-scale Vision language backbones including CLIP ViT-L/14 by OpenAI Radford et al. (2021) and Open-CLIP ViT-L/14 Cherti et al. (2023) with CIFAR-10C/100C as D_d and MNIST, SVHN, Tiny-ImageNet and CIFAR-100C/10C as D_u. From Table 14, we observe that ROSITA consistently outperforms even very recent baselines like (K+1)PC Li et al. (2023), TDA Karmanov et al. (2024), suggesting that the performance of ROSITA is agnostic to the choice of VL backbone.

Table 14: Comparison of ROSITA with prior methods on large scale Vision Language backbones.

VL Backbone	Method	CIFAR-10C				CIFAR-100C			
		MNIST	SVHN	Tiny	C-100C	MNIST	SVHN	Tiny	C-10C
CLIP ViT-L/14	ZSEval	83.94	74.54	80.16	72.32	56.29	52.35	53.25	49.89
	(K+1)PC	85.43	80.60	81.65	71.90	64.14	55.18	54.53	47.90
	TDA	84.91	76.87	81.07	74.23	59.11	55.25	55.44	52.48
	ROSITA	**89.46**	**83.42**	**83.61**	**75.63**	**65.41**	**60.31**	**57.55**	**54.66**
Open-CLIP ViT-L/14	ZSEval	80.64	76.90	84.10	75.40	62.96	59.38	61.10	59.57
	(K+1)PC	85.84	82.42	84.99	75.70	70.14	63.36	60.56	59.43
	TDA	80.57	77.92	84.60	75.79	64.90	60.70	62.01	61.20
	ROSITA	**89.04**	**82.98**	**85.55**	**76.62**	**70.54**	**63.84**	**62.57**	**61.84**

D.2 Experiments using different corruption types

To evaluate the robustness of our method across different domains, we do additional experiments with *impulse noise* , *motion blur* and *jpeg compression* corruptions from the corruption categories per-pixel noise, blurring and digital transforms respectively and report the results here. From Table 15, Table 16 and Table 17, we observe that ROSITA either outperforms or at par with prior methods in most cases even on using the same set of hyperparameters. This demonstrates its robustness across a variety of corruption types.

Table 15: Results on CIFAR-10C/100C (Impulse Noise) as D_d with other D_u.

		Method	MNIST			SVHN			Tiny-ImageNet			CIFAR-100C/10-C		
			AUC ↑	FPR ↓	HM ↑	AUC ↑	FPR ↓	HM ↑	AUC ↑	FPR ↓	HM ↑	AUC ↑	FPR ↓	HM ↑
C-10C (Impulse noise)	CLIP	ZS-Eval	86.34	97.77	57.67	84.40	79.43	56.80	88.97	31.86	61.11	78.61	67.88	54.40
		TPT	86.35	97.83	59.80	84.43	79.52	58.97	88.96	31.99	64.48	78.60	68.24	56.38
		TPT-C	62.34	87.66	39.90	59.71	83.29	35.42	81.30	38.59	37.02	66.22	89.92	30.86
		ROSITA	98.87	9.43	71.31	82.85	56.82	61.03	93.36	21.47	64.47	78.69	69.45	57.87
	MAPLE	ZS-Eval	91.10	76.09	64.01	92.98	45.28	63.66	83.77	44.44	60.93	79.22	65.26	57.49
		PAlign	91.10	76.01	65.76	93.00	45.13	65.28	83.78	44.42	62.75	79.22	65.24	58.80
		PAlign-C	92.43	63.39	63.61	92.92	45.86	64.50	83.36	45.74	60.83	79.30	64.47	57.00
		ROSITA	98.80	6.10	71.79	95.39	28.06	72.13	84.92	45.35	65.30	80.49	65.57	61.63
C-100C (Impulse noise)	CLIP	ZS-Eval	70.48	99.17	25.08	51.12	96.44	25.69	59.90	67.18	27.72	53.51	94.97	25.16
		TPT	70.56	99.17	25.26	51.21	96.38	26.26	59.91	67.09	28.36	53.53	94.94	25.63
		TPT-C	57.65	93.07	8.71	79.28	57.07	2.74	90.40	22.60	5.71	50.26	95.34	3.26
		ROSITA	36.47	99.96	20.98	24.17	99.77	18.99	53.57	79.85	26.27	58.02	94.15	29.75
	MAPLE	ZS-Eval	69.29	89.49	33.66	81.03	73.94	34.99	49.57	84.71	26.09	57.84	94.44	29.34
		PAlign	69.31	89.54	33.74	81.05	73.98	34.96	49.60	84.63	25.81	57.84	94.48	29.53
		PAlign-C	71.14	73.63	34.38	82.08	68.24	35.11	47.27	87.87	25.95	57.79	93.54	30.73
		ROSITA	95.38	8.80	43.06	80.25	41.21	34.88	42.77	97.15	19.70	49.73	96.72	12.62

Table 16: Results on CIFAR-10C/100C(Motion blur) as D_d with other D_u.

		Method	MNIST			SVHN			Tiny-ImageNet			CIFAR-100C/10-C		
			AUC ↑	FPR ↓	HM ↑	AUC ↑	FPR ↓	HM ↑	AUC ↑	FPR ↓	HM ↑	AUC ↑	FPR ↓	HM ↑
C-10C (Motion blur)	CLIP	ZS-Eval	97.73	2.75	73.69	96.40	18.34	73.82	95.25	15.75	74.27	79.57	70.08	62.86
		TPT	97.72	2.68	74.15	96.39	18.16	74.42	95.23	15.72	75.03	79.56	69.86	63.25
		TPT-C	80.73	86.28	63.74	62.09	62.52	42.19	80.76	51.66	48.04	55.66	97.04	37.53
		ROSITA	99.90	0.04	81.87	96.50	21.55	77.47	96.58	13.65	77.44	82.03	65.95	66.96
	MAPLE	ZS-Eval	96.52	18.33	78.68	97.08	14.78	78.15	88.45	33.15	71.19	84.00	57.94	66.93
		PAlign	96.51	18.37	78.92	97.08	14.82	78.38	88.45	33.13	71.73	83.99	57.99	67.15
		PAlign-C	97.17	13.47	78.49	96.89	15.87	78.09	88.80	32.94	72.09	84.29	56.80	67.40
		ROSITA	98.49	10.01	83.26	92.61	44.87	78.93	87.48	38.23	73.24	84.27	57.60	70.67
C-100C (Motion blur)	CLIP	ZS-Eval	93.08	58.92	48.17	83.63	81.33	46.04	79.34	53.56	48.53	64.03	91.54	41.63
		TPT	93.06	59.87	48.18	83.61	81.56	45.54	79.29	53.76	48.26	64.02	91.63	41.25
		TPT-C	66.77	98.77	19.96	29.69	99.94	11.39	69.25	62.87	17.10	53.22	94.57	13.59
		ROSITA	98.93	6.79	55.49	89.39	37.86	48.50	90.20	31.61	55.05	65.30	91.59	42.54
	MAPLE	ZS-Eval	81.21	80.28	45.66	89.04	60.73	46.98	60.84	80.63	40.60	64.01	90.18	42.30
		PAlign	81.20	80.52	44.52	89.03	61.01	45.76	60.84	80.64	40.03	64.01	90.26	41.26
		PAlign-C	82.72	68.08	49.92	90.48	53.83	51.87	62.00	82.85	41.66	64.47	89.05	43.58
		ROSITA	97.12	7.78	57.30	85.13	56.16	49.89	63.85	80.20	42.65	62.55	94.62	41.54

Table 17: Results on CIFAR-10C/100C(JPEG Compression) as D_d with other D_u.

		Method	MNIST			SVHN			Tiny-ImageNet			CIFAR-100C/10-C		
			AUC ↑	FPR ↓	HM ↑	AUC ↑	FPR ↓	HM ↑	AUC ↑	FPR ↓	HM ↑	AUC ↑	FPR ↓	HM ↑
C-10C (JPEG)	CLIP	ZS-Eval	68.16	100.00	53.92	67.04	99.93	55.69	79.44	65.02	59.66	73.65	85.60	56.30
		TPT	68.07	100.00	54.16	66.97	99.93	56.06	79.37	65.11	60.09	73.64	85.58	56.87
		TPT-C	68.28	99.37	53.12	54.76	98.97	35.64	66.70	72.20	39.02	59.82	94.78	32.78
		ROSITA	81.83	58.81	60.34	82.85	61.38	61.87	95.06	15.84	67.87	71.19	86.62	51.98
	MAPLE	ZS-Eval	95.15	33.39	69.72	95.96	22.02	69.73	86.64	36.79	65.68	79.26	68.19	60.10
		PAlign	95.13	33.57	69.62	95.95	22.01	69.31	86.63	36.82	65.62	79.26	68.18	59.86
		PAlign-C	96.53	20.14	70.50	95.94	21.51	70.01	87.38	35.07	66.42	79.85	66.17	61.11
		ROSITA	99.28	5.71	76.74	95.54	29.06	72.86	89.88	31.12	68.78	80.69	61.64	62.23
CIFAR-100C (JPEG)	CLIP	ZS-Eval	50.88	100.00	32.27	39.25	100.00	26.41	48.65	95.60	29.92	53.51	95.59	32.48
		TPT	50.78	100.00	32.38	39.18	100.00	26.48	48.55	95.60	29.86	53.49	95.57	32.70
		TPT-C	12.11	100.00	3.32	10.05	99.98	2.45	63.07	90.01	9.49	52.23	95.05	6.33
		ROSITA	29.10	100.00	22.83	35.58	99.94	23.50	50.76	94.76	31.64	53.96	96.18	30.39
	MAPLE	ZS-Eval	78.86	80.60	37.60	87.72	61.14	39.18	58.31	80.75	34.03	54.50	95.49	34.02
		PAlign	78.82	80.92	36.62	87.69	61.37	38.01	58.29	80.79	33.17	54.49	95.52	32.96
		PAlign-C	81.85	63.37	40.87	89.96	49.09	41.89	59.33	81.48	33.84	53.82	95.17	33.28
		ROSITA	97.68	7.87	46.51	92.14	34.44	42.71	66.63	75.00	37.43	51.33	96.68	25.41

D.3 Open Set Single Image CTTA Experiments

Here, we report the detailed corruption-wise results presented in Table 5. In addition, we evaluate the performance of ROSITA in comparison with prior methods more extensively here. We present the 15 corruptions of CIFAR-10C sequentially as D_d, one sample at a time along with different datasets for C_u samples, namely MNIST, SVHN, Tiny ImageNet, CIFAR-100C and report the results in Table 18. We observe that the improvement in performance of ROSITA is agnostic to model architecture, challenging scenarios including different combinations of D_d (continuously changing domains) and D_u datasets.

Table 18: Results on Openworld Single Image Continuous Test Time Adaptation(CTTA) for CIFAR-10C (15 corruptions shown sequentially) as D_d with other D_u datasets.

		Method	*gaussian*	*shot*	*impulse*	*defocus*	*glass*	*motion*	*zoom*	*snow*	*frost*	*fog*	*brightness*	*contrast*	*elastic*	*pixelate*	*jpeg*	Mean
CIFAR-10C/MNIST	CLIP	ZS-Eval	43.21	47.74	57.68	75.43	38.56	73.91	76.94	75.56	79.38	74.36	84.88	67.36	55.61	60.56	53.82	64.33
		TPT	43.15	47.66	**57.70**	75.36	38.22	73.70	76.84	75.49	79.32	74.80	84.82	67.46	55.50	60.40	53.48	64.26
		TPT-C	30.06	25.92	31.05	52.71	20.88	45.97	53.08	21.61	26.83	38.80	38.88	37.40	33.83	35.26	3.53	33.05
		ROSITA	**43.35**	**48.21**	57.04	**78.01**	**43.29**	**77.48**	**80.16**	**76.84**	**80.15**	**76.26**	**86.33**	**73.44**	**60.35**	**61.55**	**60.38**	**66.86**
	MAPLE	ZS-Eval	42.33	44.71	64.00	78.78	45.90	78.69	81.12	82.56	84.79	78.13	88.87	67.94	63.87	51.63	69.77	68.21
		PAlign	42.95	44.22	64.85	77.36	44.70	78.44	80.16	82.46	83.47	77.25	88.29	65.49	64.34	51.73	67.53	67.55
		PAlign-C	42.97	45.32	63.98	78.79	48.07	78.42	81.09	83.88	85.21	77.38	89.09	69.90	66.22	56.59	70.01	69.13
		ROSITA	**43.51**	**49.92**	**64.87**	**78.98**	**54.56**	**80.58**	**84.04**	**87.27**	**89.09**	**84.11**	**93.02**	**78.60**	**74.02**	**71.64**	**75.30**	**73.97**
CIFAR-10C/SVHN	CLIP	ZS-Eval	42.86	47.15	56.79	75.11	41.57	74.03	76.65	74.07	77.73	73.66	83.01	68.03	54.80	59.66	55.58	64.05
		TPT	42.82	47.10	56.82	74.98	41.49	73.88	76.64	74.05	77.67	73.93	82.95	68.32	54.70	59.60	55.51	64.03
		TPT-C	37.26	34.53	39.45	62.23	30.72	55.30	62.65	45.74	47.70	50.35	55.42	57.01	43.26	45.32	29.64	46.44
		ROSITA	**43.08**	**47.99**	**57.62**	**76.73**	**42.35**	**74.99**	**78.59**	**76.34**	**78.54**	**72.00**	**83.58**	**68.93**	**60.21**	**60.08**	**57.86**	**65.26**
	MAPLE	ZS-Eval	45.34	50.19	63.65	78.24	52.00	78.13	80.62	83.57	85.00	77.77	88.80	67.55	63.51	55.23	69.73	69.29
		PAlign	**45.74**	50.29	64.35	76.99	51.50	77.97	79.89	83.16	83.63	76.89	88.47	65.56	64.10	55.91	67.70	68.81
		PAlign-C	45.36	50.36	63.83	78.19	51.55	77.84	80.50	83.05	84.42	76.82	88.15	71.57	65.50	55.01	70.04	69.48
		ROSITA	45.51	**50.99**	**64.73**	**78.36**	**53.10**	**78.74**	**80.87**	**83.79**	**85.18**	**78.47**	**88.71**	**70.78**	**66.70**	**59.28**	**71.18**	**70.43**
CIFAR-10C/Tiny	CLIP	ZS-Eval	49.41	52.96	61.09	76.40	49.23	74.28	77.36	74.49	77.39	73.92	81.34	70.26	60.29	59.40	59.67	66.50
		TPT	49.43	52.97	61.07	76.41	49.13	74.27	77.36	74.63	77.43	74.05	81.49	70.14	60.16	59.28	59.66	66.50
		TPT-C	49.64	51.56	59.10	74.35	47.37	66.65	71.56	60.46	62.19	63.91	69.60	63.85	55.65	52.31	42.58	59.38
		ROSITA	**49.64**	**53.56**	**61.64**	**77.02**	**50.23**	**76.09**	**79.22**	**78.05**	**79.34**	**76.84**	**84.55**	**73.65**	**65.87**	**58.86**	**68.76**	**68.89**
	MAPLE	ZS-Eval	44.18	47.30	60.94	71.71	49.99	71.18	73.40	76.15	76.76	71.56	80.22	64.44	61.51	55.67	65.69	64.71
		PAlign	44.17	46.35	61.56	70.27	48.90	70.63	72.46	75.57	75.32	70.66	79.65	62.53	62.15	56.28	63.13	63.98
		PAlign-C	**44.38**	**48.00**	61.09	72.15	49.94	72.06	74.47	76.10	**77.67**	72.13	80.51	66.68	61.75	55.69	66.51	65.28
		ROSITA	44.29	47.93	**61.59**	**72.35**	**51.11**	**72.20**	**74.47**	**76.34**	77.45	**72.89**	**80.82**	**66.70**	**62.81**	**57.72**	**67.00**	**65.71**
CIFAR-10C/CIFAR-100C	CLIP	ZS-Eval	40.48	44.50	54.34	67.17	40.46	62.85	68.16	68.90	70.68	65.22	76.26	62.16	51.48	48.42	56.23	58.49
		TPT	40.43	44.45	54.32	67.13	40.40	62.89	68.14	68.90	70.71	65.17	76.24	62.13	51.41	48.46	56.31	58.47
		TPT-C	27.80	26.46	33.01	40.72	28.05	38.78	42.05	41.90	43.91	39.15	45.80	41.50	37.11	32.71	39.69	37.24
		ROSITA	**40.66**	**45.15**	**55.01**	**67.31**	**41.07**	**63.12**	**68.54**	**69.58**	**71.09**	**66.23**	**76.34**	**63.89**	**54.15**	**48.23**	**57.08**	**59.16**
	MAPLE	ZS-Eval	41.99	45.82	57.50	69.19	44.03	66.86	70.43	**71.81**	**73.33**	68.32	76.95	64.18	56.74	49.81	60.15	61.14
		PAlign	41.93	45.16	57.81	68.04	42.44	66.54	69.56	71.35	71.78	67.46	76.70	62.17	56.98	49.86	58.22	60.40
		PAlign-C	41.86	45.80	57.51	69.78	46.17	**67.73**	**71.47**	71.03	74.00	68.98	77.61	65.53	57.08	52.17	61.17	61.86
		ROSITA	**42.13**	**46.09**	**58.00**	**69.48**	**45.33**	67.44	71.00	71.00	73.31	**69.42**	**78.37**	**65.55**	**57.32**	**53.52**	**60.85**	**61.92**